CARBON NANOSTRUCTURES GROWN ON 3-D SOLID STRUCTURES FOR DRY REFORMING OF METHANE

BY

Saheed Adewale Ganiyu

A Thesis Presented to the
DEANSHIP OF GRADUATE STUDIES

KING FAHD UNIVERSITY OF PETROLEUM & MINERALS
DHAHRAN, SAUDI ARABIA

In Partial Fulfillment of the
Requirements for the Degree of

MASTER OF SCIENCE
In

CHEMISTRY DEPARTMENT

May 2013

KING FAHD UNIVERSITY OF PETROLEUM & MINERALS

DHAHRAN- 31261, SAUDI ARABIA

DEANSHIP OF GRADUATE STUDIES

This thesis, written by **Saheed Adewale Ganiyu** under the direction of his thesis advisor and approved by his thesis committee, has been presented and accepted by the Dean of Graduate Studies, in partial fulfillment of the requirements for the degree of **MASTER OF SCIENCE IN CHEMISTRY.**

Thesis Committee

Dr. Khalid R. Alhooshani
(Advisor)

Dr. Abdullah J. Al-Hamdan
Department Chairman

Dr. Oki Muraza
(Member)

Dr. Salam A. Zummo
Dean of Graduate Studies

Dr. Nisar Ullah
(Member)

25/7/13
Date

DEDICATED

IN LOVING MEMORY OF MY LATE FATHER

ACKNOWLEDGMENTS

Glory is to Allah, the lord of the Mankind, who made my existence on the surface of the Earth a real one and guides me throughout the programme.

My profound gratitude goes to my advisor, Dr. Khalid R. Al-Hooshani and the Thesis committee, Dr. Nisar Ullah and Dr. Oki Muraza for their unquantifiable supports in all ramifications throughout the period of my research.

I would like to express my sincere appreciation to Dr. Zain H. Yamani, Director Centre of Excellence Nanotechnology for his moral and professional supports, and for the opportunity given me to serve and operate effectively as a Research Assistant in the Centre. In the same vein, my appreciation extends to all Research Scientists and members of the Centre, especially the Assistant Lab. Manager, Dr. Nasir Zaman and Dr. Abbas Saeed for quality images analysis and technical discussion.

I would like to acknowledge the efforts of Dr. Muataz, Mr. Dan and Mr. Jerwin, in providing CVD-reactor and training for my research.

I am indeed grateful to king Fahd University of Petroleum and Minerals (KFUPM) for opportunity given me to pursue my M.Sc. Degree through scholarship.

My sincere appreciation also goes to Nigerian community and African community at large for their hospitality.

I would like to acknowledge the financial support of the National Science, Technology and Innovation Plan (NSTIP), through project number (10-NAN1391-04).

This remains incomplete without acknowledging the supports of my extended and immediate family, especially my dear wife and little son, Abdullah for their patience and endurance during the course of my M.Sc. program.

Thank you all for your supports.

TABLE OF CONTENTS

LIST OF TABLES

LIST OF FIGURES

LIST OF ABBREVIATIONS

CNSs	:	Carbon Nanostructures
CNFs	:	Carbon Nanofibres
SiC	:	Silicon-Carbide
C-TCVD	:	Catalytic-Thermal Chemical Vapour Deposition
FESEM	:	Field Emission Scanning Electron Microscope
XRD	:	X-Ray Diffraction
SWNTs	:	Single Wall Nanotubes
MWNTs	:	Multi Wall Nanotubes
CVD	:	Chemical Vapour Deposition
PPI	:	Pores per Inch
SMSI	:	Strong Metal-Support Interaction
DRM	;	Dry Reforming of Methane
SR	:	Steam Reforming
TEOS	:	Tetra Ethyl Ortho-Silicate
EISA	:	Evaporation Induced Self-Assembly
CTAB	:	Cetyl Trimethyl Ammonium Bromide
IWI	:	Incipient Wetness Impregnation
BET	:	Brunner Emmet Teller
TEM	:	Transmission Electron Microscope
SE	:	Secondary Electron
BSE	:	Back-Scattered Electron
CCD	:	Charged Couple Device

TOS	:	Time on Stream
WSGR	:	Water Shift Gas Reaction
DFT	:	Density Function Theory

ABSTRACT

Full Name : Saheed Adewale Ganiyu

Thesis Title : Carbon Nanostructures Grown on 3-D Solid Structure for Dry Reforming of Methane

Major Field : Chemistry

Date of Degree : May 2013.

Mass and heat transfer limitations in heterogeneous catalysis could lead to the loss of catalyst activity and selectivity, which in turn lower the reaction rates and lead to poor yield with high unwanted by-products. In order to improve mass and heat transfer rates, a novel catalyst support with high surface area, better oxidation and corrosion resistance, high chemical and thermal stability, porous materials with high surface area to volume ratio, low mass density, and high thermal conductivity is required.

In this present work, carbon nanostructure in form of carbon nanofibers (CNFs) and carbon nanobulbs (CNBs) of different diameters have been grown between 600-900^{o}C on 3-D silicon carbide (SiC) with the aid of interfacial oxide by using catalytic thermal chemical vapor deposition method (C-TCVD).

Textural properties were characterized by FESEM, TEM, XRD, RAMAN, and N_2 gas adsorption-desorption, to examine and determine the size, microstructure, morphology, surface area, pore volume, crystallinity, and the degree of graphitization of CNSs.

The as-grown CNFs at 700^{o}C on 3-D SiC-foam with high specific surface area of 182 m^2/g and high degree of graphitization was evaluated for dry reforming of methane at 800^{o}C using (CH_4 and CO_2, 1:1) to produce syn-gas of different ratios.

ملخص الرسالة

الاسم الكامل: سَهيد عدولي غنيو

عنوان الرسالة: تطوير بنى-نانونية كاربونية في وجود بنية صلبة ثلاثية الابعاد من اجل اعادة التكوين الجاف لغاز الميثان

التخصص: الكيمياء

تاريخ الدرجة العلمية: مايو 2013

ان معوقات انتقال المادة والحرارة لدى الحفازات المتجانسة ربما يؤدي الى فقدان الفعالية والخاصية المسامية, وهذا بالاخير يؤدي الى إنخفاض في معدل التفاعل مما يجعل الإنتاجية ضئيلة وانتاج مواد ثانوية غير مرغوبه. من أجل تحسين معدل انتقال المادة والحرارة: حفازات حديثه ذات مساحة سطح عالية و مقاومة افضل للتأكسد والتآكل و استقرار حراري وكيميائي عالي , ومواد مسامية ذات مساحة سطح عالية بالنسبة للحجم , ومنخفضة الكثافة وذات خاصية توصيل حراري عالي هو الهدف المطلوب.

في هذا العمل الحالي, بنية- ناونونيه كاربونية على شكل ألياف نانونية كربونية (CNFs) وكرات نانونية كاربونية ذات اقطار مختلفة تم تصنيعها عند درجة حرارة تتراوح مابين 600 الى 900 درجة مئوية على كربيد السيليكون ثلاثي الأبعاد في وجود أوكسيدات بينية بإستخدام ترسيب المحفز الكيميائي الحراري البخاري (C-TCVD) . تم التعرف على الخصائص التكوينية بواسطة الاشعة السينية (XRD) و المجهر الالكتروني الماسح (FESEM) و رامان(RAMAN) و تي إي أم (TEM), و عملية امتصاص-انتزاع النيتروجين لتحديد و اختبار الحجم والبنى المجهرية و شكل و مساحة السطح و حجم المسام و درجة التبلور ودرجة تكوَن جرافيت الـ CNSs .

إن مادة .CNFs المطورة على رغوة كربيد السيليكون عند درجة حرارة 700 درجة مئويه, بمساحة سطح عالية (182 م^2 /جرام) و درجة جرافيتية عالية , قد تم إختبارها في الإصلاح الجاف للميثان عند 800 درجة مئوية بإستخدام الميثان وثاني اكسيد الكاربون بنسبة 1:1 من اجل انتاج syn-gas عند نسب مختلفه.

CHAPTER 1

INTRODUCTION

1.1 Carbon and its Allotropes

Existence of carbon was dated to prehistoric times in the form of charcoal and soot. In the year 1797, the English chemist Smithson Tennant proved that diamond is pure carbon. It is found in abundance in the sun, stars, comets, and atmospheres of most planets [1].

Naturally occurring allotropes of carbon are diamond, graphite and amorphous, but no specific consensus about how many allotropes exists. Others allotropes include white carbon, buckingminster fullerenes, and different carbon nanostructures such as carbon nanofoam, nanobud, nanotubes and nanofibers [2-5].

Graphite is Sp^2 hybridized, exists in alpha and beta form and produced by heating coke in an oxygen-free furnace at 3500^oC, while diamond is Sp^3 produced by squeezing graphite under high temperatures and pressures [1].

1.2 Discovery of Carbon nanostructures

The popular stories about carbon nanostructures did not begin until 1985 when buckinminster fullerenes or buckyballs (fig 1.1) were discovered in 1985 in molecular beam experiments by Harold W. Kroto (University of Sussex), Robert F. Curl and Richard E. Smalley (Rice University), three of whom were awarded the 1996 Nobel Prize in Chemistry. Fullerenes Composed of honeycomb type lattices of hexagons

and pentagons molecules, composed entirely of carbon, which could be hollow sphere, ellipsoid, or tube [5].

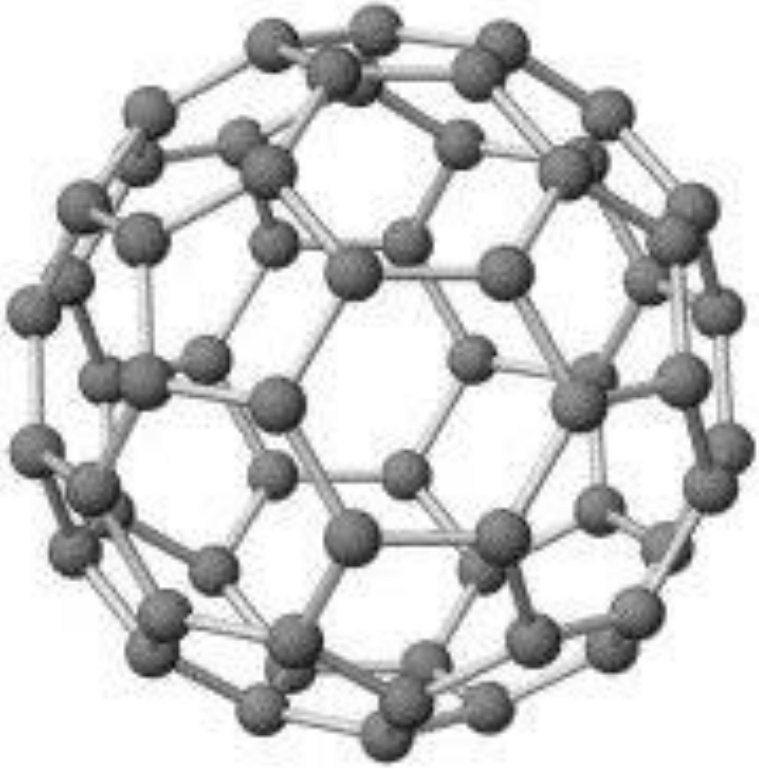

Fig.1.1: Fullerenes buckinminster.

Aftermath buckinmister discovery, an electron microscopist Sumio Iijima in 1991 discovered fullerene-related carbon nanotubules (bucky tubules) in an arc discharge evaporation, due to earlier motivational work from kratchmer-Huffman on carbon soot. Since then different forms of carbon nanofilaments including carbon nanocones, carbon nanohorns, nanoscale carbon toroidal structures and helicoidal tubes, periodical carbon structures Schwarzites and Haeckelites, have been discovered [6-10].

Three distinct structural types of filaments have been identified based on the graphene layers with respect to filament axis, namely stacked, herringbone (or cup-stacked) and nanotubular [11].

Carbon nanofibers have been long known as nuisance in catalytic conversion of carbon-containing gases. This graphitic nanostructure (3-100nm diameter, 0.1-1000μm length) has unique properties with fullerenes and carbon nanotubes, and has attracted great research interests in different area of applications [12].

1.3 Synthesis Techniques of Carbon Nanostructures

Arc discharge, laser ablation and chemical vapor discharge, are three popular methods of synthesizing CNSs up to date.

Arc discharge was first used by Vasily V. Petrov, a Russian scientist in 1802 as a special fluid with electrical properties, while experimenting copper-zinc battery consisting of 4200 discs [13] . This method was used initially for fullerenes carbon before discovery of carbon nanotubes in 1991.

It involves application of direct-current arc voltage (5-100amp, 20V) across two graphite electrodes at high temperature of 2000-3000^{o}C, immersed in an inert gas such as He, N_2 or water to vaporize carbon. When pure graphite rods are used, fullerenes are deposited as soot inside the chamber, and multi-walled carbon nanotubes are deposited on the cathode. When a graphite anode containing a metal catalyst (Fe or Co) is used with a pure graphite cathode single-walled carbon nanotubes are generated in the form of soot [14].

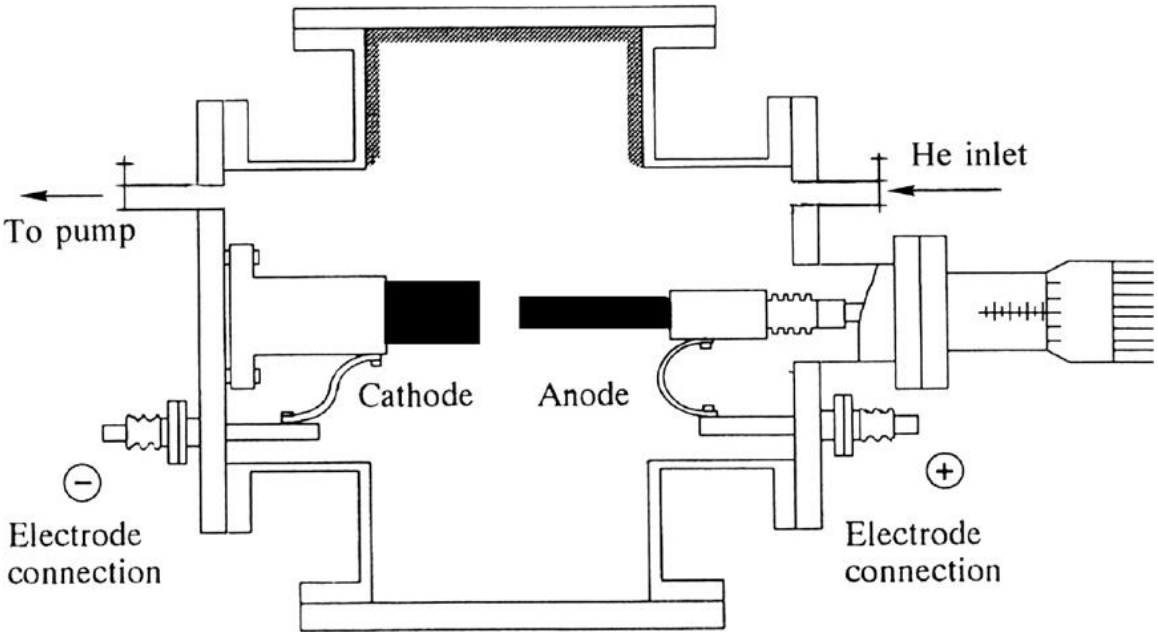

Fig.1.2: Schematic diagram of arc-discharged equipment [15].

Laser ablation is the process of removing material from a solid (or occasionally liquid) surface by irradiating it with a laser beam. At low laser flux, the material is heated by the absorbed laser energy and evaporates or sublimates. At high laser flux, the material is typically converted to a plasma. Usually, laser ablation refers to removing material with a pulsed laser, but it is possible to ablate material with a continuous wave laser beam if the laser intensity is high enough.

This technique can be used to produce carbon nanostructure, MWNTs and SWNTs with or without addition of metal catalyst respectively, by vaporizing carbon from graphite target at high temperature. The quantity and quality of produced carbon nanotubes depend on several factors such as the amount and type of catalysts, laser power and wavelength, temperature, pressure, type of inert gas, and the fluid dynamics near the carbon target [16, 17].

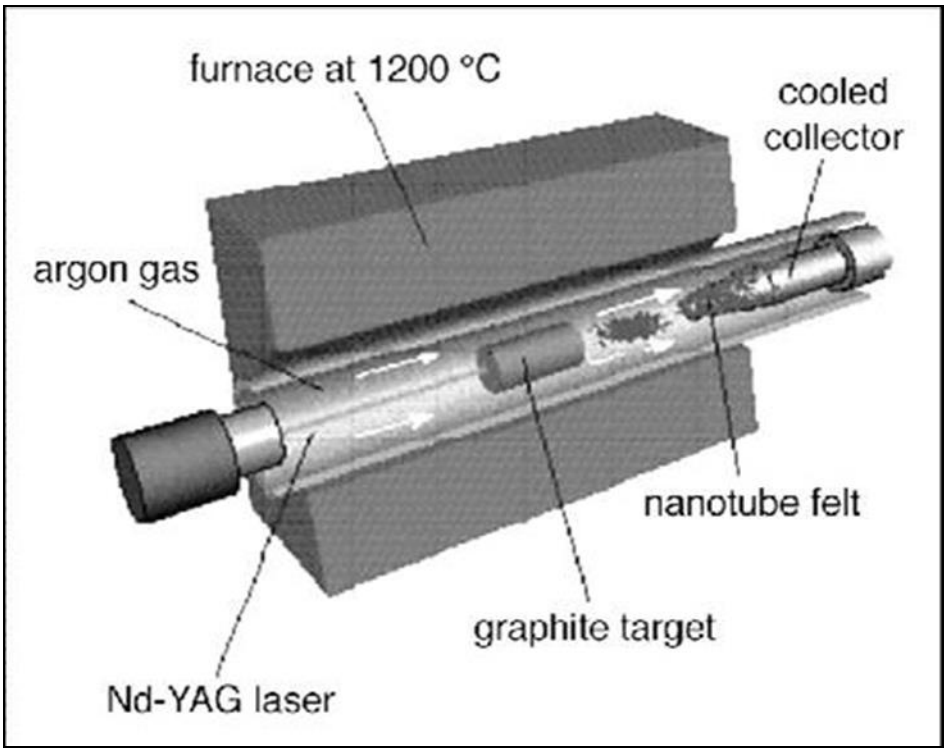

Fig.1.3: Oven laser-ablation equipment [16].

The Catalytic-thermal chemical vapor deposition (C-TCVD) technique received more popularity than above-mentioned two techniques due to its ease operation and potential for industrial large-scale production.

The growth process involves a catalyst material at high temperature in a tube furnace and a hydrocarbon gas flowing through the tube reactor for a period. Materials grown over the catalyst are collected upon cooling the system to room temperature. The key parameters in CVD growth of CNSs are the hydrocarbons, catalysts and growth temperature. The active catalytic species are typically transition-metal nano-particles formed on a support material such as alumina, silica and so on [18, 19].

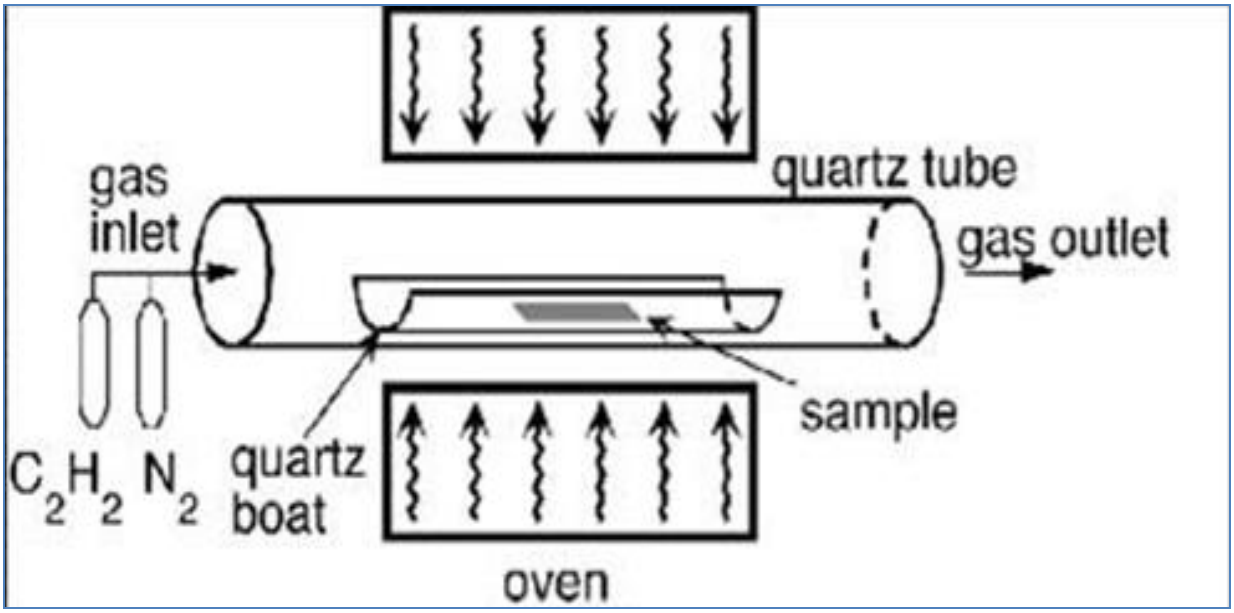

Fig.1.4: Schematic representation of chemical vapor deposition equipment.

1.4 Excellent Properties of CNSs Compared to other Leading Materials

- CNSs have 100GPa tensile strength compared to steel 2GPa
- 48,000 KN·m·kg^{-1} specific strength compared to high steel 154 KN·m·kg^{-1}.
- Current capacity of 1GAmps / cm^2 compared to Copper wire 1MAmps / cm^2.
- Young Modulus (stiffness) 1250 GPa compared to High strength steel 200 GPa
- High thermal conductivity Compared to pure diamond (3320 W / m.K) [20-23].

1.5 Carbon Nanostructures Growth Mechanism

Generally, proposed mechanism by various researchers in the formation of CNS involves simplified three steps; (i) adsorption and decomposition of carbon-containing gas on the exposed surface of active catalyst site to deposit carbon and release hydrogen, (ii) dissolution of carbon in the metal particle to form metal-carbide, and (iii) diffusion of the dissolved carbon through the metal particle and precipitation/growth of CNS at the other end of the particle [24, 25].

Hydrocarbon decomposition is exothermic step that evolves heat to the exposed catalyst surface, while carbon crystallization being endothermic absorbs heat from metal precipitation zone. The growth process is continuous due to precise thermal gradient within the active phase particle.

There are two-growth observable pattern of CNS on metal particle; when catalyst-substrate interaction is weak, the hydrocarbon decomposes and diffuses down the metal particle and CNS precipitates out across the metal bottom, pushing the completely metal particle off the substrate. The growth continues as long as the top of the metal is open for

fresh hydrocarbon decomposition, the concentration gradient exists in the metal allowing carbon diffusion, and CNS continues to grow longer until the metal is fully covered with carbon, this is known as tip-growth model [26]

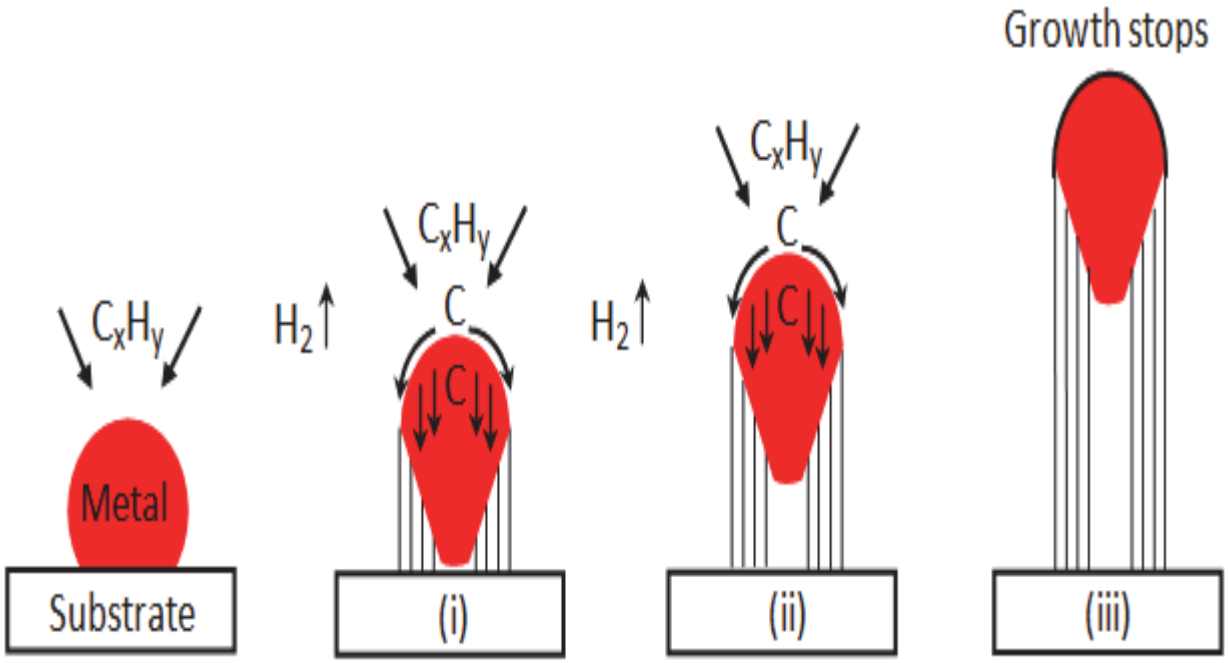

Fig.1.5: Schematic representation of tip-growth mechanism.

On the other hand, when the substrate-metal interaction is strong, the initial hydrocarbon decomposition and carbon diffusion take place similar to that in the tip-growth case but CNS precipitation fails to push the metal particle up; so the precipitation is compelled to emerge out from the metal's top. Carbon crystallizes out as a hemispherical dome that then extends up in the form of seamless graphitic cylinder and the subsequent hydrocarbon decomposition takes place on the lower part of the metal, and as-dissolved carbon diffuses upward. This is known as "base-growth model" [26].

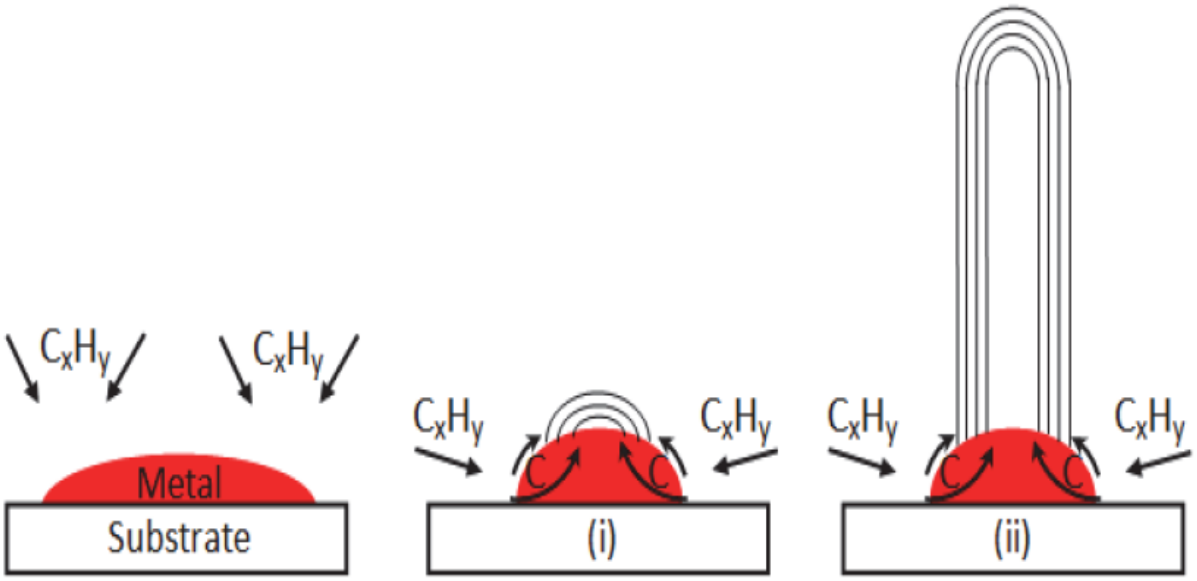

Fig.1.6: Schematic diagram of base growth mechanism of CNSs

1.6 Method of Catalyst Preparation

Catalyst preparation has been described as a “black art” and can be classified into three broad categories with respect to the preparation procedure: (i) Bulk catalysts and supports; (ii) Impregnated catalysts; (iii) Mixed-agglomerated catalysts [27].

Bulk catalysts are mainly comprised of active substances. Important examples include silica alumina for hydrocarbon cracking, Zn-Cr oxide catalyst for the conversion of CO-H_2 mixtures to methanol, iron-molybdate for methanol oxidation. The supports are prepared by similar procedures (e.g. alumina, silica and silica alumina).

Impregnated catalysts are usually obtained from preformed supports by impregnation with the active phase; most of hydrogenation catalysts are prepared in this way.

The mixed-agglomerated catalysts comprises of those catalysts obtained by mixing the active substances with a powdered support or a support precursor and then agglomerating the mixture [28].

Catalyst preparations routes to be employed may include; impregnation (by excess solution or wet incipient), ion exchange, precipitation, sol-gel method, organometallic grafting, gas phase deposition, solid-solid reaction and wash coating, and each route involve several steps. Many supported metal and oxides are prepared by the succession of impregnation, drying, calcination, and activation, while zeolites catalysts are prepared by precipitation of gel, crystallization, washing, ion exchange and drying [29].

1.7 Objectives

- To synthesize and deposit mesoporous interfacial oxide layer on 3-D solid foam support.
- To evaluate the potential of two different metal catalysts (Ni and Fe) in uniform growing of CNSs at different temperatures (600-900^{o}C) on 3-D SiC solid support.
- To evaluate the quality and uniform distribution of carbon nanostructures by applying different characterization techniques.
- To evaluate the potential of synthesized carbon nanostructures for dry reforming of methane.

CHAPTER 2

LITERATURE REVIEW

2.1 Silicon Carbide Foam as a Support in Catalysis

Foams (ceramic or metal) are defined as materials containing gaseous voids surrounded by a liquid or solid denser matrix [30].

Owing to their remarkable properties such as large external surface area, a high mechanical strength, a high porosity and a low resulting pressure drop, low heat transfer rate, high temperature resistance, corrosion resistance and excellent acoustic property, foams have been employed for various industrial applications including thermal insulation, packaging, absorbents and structural uses, but emerging applications include catalysis and water cleaning [31, 32].

Ceramic foams have a sponge-like structure with pore densities of usually 10–100 PPI (pores per inch) and a typical porosity range of 75–90% [33].

Ceramic foams can be manufactured by different methods, e.g. replication techniques, direct foaming techniques, Hollow beads method etc. Most commercial ceramic foams are produced by applying replication techniques in which they are obtained as positive image of the polymeric foam template. In this technique, polymeric sponge is coated with ceramic slurry, dried, calcined and sintered [34-37].

The first commercial application of Ceramic foam reported in the literature as filters for molten metals. SiC-foam is ceramic cellular foam that composed of a three-dimensional network of struts, with many applications as filters for molten metal, hot gas and diesel

engine exhausts filters, catalyst carriers, biomaterials, thermal insulators for furnaces and aerospace applications, gas combustion burners and lightweight building materials.

In catalysis, specific surface area and pressure drop properties of foam catalyst supports are extremely important parameter to evaluate catalytic efficiency. As a catalyst support, ceramic foams offer a combination of attractive properties such as low-pressure drop, good chemical resistance and enhanced heat and mass transfer [38, 39].

2.2 Carbon Nanostructures for Catalytic Application

Since its discovery in 1991 by Iijma, [3] carbon nanostructures with a variety of novel properties, such as high specific modulus, good mechanical strength, high surface area, chemical and thermal stability, low mass density, and high electric conductivity [40], have been attracting great interest in different field of applications, including catalysts and catalysis, adsorbents, capacitors, nanosensors, hydrogen storage, and performance-enhanced hybrids materials [41-43].

Recently, intensified efforts have been shifted towards application of nanostructure on solid supports in heterogenous catalysis, due to major challenges commonly encountered in the development of catalytic layers for structured catalysts and structured reactors, which include: (i) to incorporate large surface area materials to encounter low catalyst loading and incorporation of active nanoparticles, (ii) to develop thicker films up to the critical thickness to avoid internal diffusion limitations (iii) to provide high accessibility of active nanoparticles for the reactants, (iv) to improve a long term stability of the nanoparticles during the reaction and (v) to have flexibility on having tunable surface properties. (viz. inert, acidity or basicity).

Carbon nanofibers (CNFs) (entangled or forest form), are promising graphitic catalysts and catalysts supports [12, 44-46] for wide applications in heterogenous catalysis applications. Carbon nanostructures such as CNFs and CNTs are inert catalyst support where acidity and strong metal-support interactions (SMSI) are not required and have advantages over acidic catalysts such as alumina and zeolites. Though alumina is a widely used catalyst support, there are many efforts to find alternative catalyst supports.

The SMSI between the active metal nanoparticles and the alumina support reduce the available fraction of metal for the reaction, which consequently reduces catalyst activity. Alumina is also chemically reactive and under certain reaction conditions, secondary solid-solid interaction may occur between the alumina support and the deposited metal active phase leading to the active phase lost [47]. It is also important to note that the chemical inertness of the SiC-based supports allows one to envisage the recovery of both the active phase and the support after the end-life of the catalyst by a simple acid or basic treatment. Such recovery task cannot be applied for the traditional supports such as alumina or silica. It is expected that the possibility to recover the active phase and the support will significantly reduce the input cost of the process.

2.3 Dry Reforming of Methane with Carbondioxide

Due to Industrial Revolution, human activities such as burning of fossil fuels (oil, coal and gas) and deforestation, have greatly increased CO_2 emission concentrations in the atmosphere by 25% compared to pre-industrial era. In 2010, 9.14 gigatonnes of carbon (33.5gigatonnes of CO_2) were released from fossil fuels and cement production worldwide, compared to 6.15 gigatonnes in 1990 [48].

Thus, it is of great importance to reduce the emission of CO_2 into the air due to global warming effect of this Greenhouse gas. Different attempts made include, disposal of CO_2 by using low-carbon containing natural gas fuel instead of heavy fuel source like naphtha which produces high, Capturing, sequestration and disposal, and fixation into economic value chemicals such as carbamic esters, Urea, & methylamines etc. [49].

There are various ways of Mitigating CO_2 to yield valuable/economic chemicals such as synthesis of urea (for nitrogen fertilizers and plastics), salicylic acid (a pharmaceutical ingredient), and polycarbonates (for plastics) [50] and CO_2 dry reforming.

Dry reforming of methane offers a potential way of reducing global warming by consumption of CO_2 and CH_4, which are two important greenhouse gases, and their conversion to syn-gas (Eq. 1) gives this process a great interest for environment protection [40, 43, 47, 51] and natural gas valorization. Another advantage of this process is the production of CO-rich syngas, which is considered as feedstock to produce many oxygenated hydrocarbons as methanol and dimethyl ether and so on [12, 25].

$$CH_{4\,(g)} + CO_{2\,(g)} \rightarrow 2CO_{(g)} + 2H_{2\,(g)} \qquad \Delta H_{298\,K} = 247{:}0\ kJ/mol \quad (1)$$

$$CH_{4\,(g)} + H_2O_{(l)} \rightarrow CO_{(g)} + 3H_{2\,(g)} \qquad \Delta H_{298\,K} = 206{:}4\ kJ/mol \quad (2)$$

Synthesis gas is traditionally produced by highly endothermic steam reforming of natural gas to produce H_2/CO ratio (>3) equation (2), which is not viable for Fischer–Tropsch, methanol and other oxygenated products syntheses. Thus, research efforts have been directed towards obtaining syn-gas with a more suitable H_2/CO ratio of unity *via* methane partial oxidation or by CH_4/CO_2 reforming or auto-thermal oxidation [52].

Partial oxidation of methane and CO_2 reforming of methane have the potential to reduce the cost of syngas and/or CO_2 utilization technologies [53].

$$CH_{4\,(g)} + 1/2O_{2\,(g)} \rightarrow CO_{(g)} + 2H_{2\,(g)} \qquad \Delta H^{o}_{298} = -38KJ/mol \quad (3)$$

The DR process becomes industrially advantageous compared to steam reforming (SR) (Eq. 2) or partial oxidation (Eq. 3) in syngas production since H_2/CO product ratio is close to 1/1, which is suitable for further use in the production of oxygenated compounds such as methanol, dimethyl ether as well as Fischer– Tropsch synthesis for production of liquid hydrocarbons.

DRM has been studied extensively on different metal catalysts such as (Rh, Ru, Ir, Pd and Pt) [54] and as well Ni on different acidic or basic supports.

Noble metals are resistance to coking and have very long stability in DRM but the cost implication and availability limit their use.

Ni is desirable due to its cost and availability compared to noble metals, but the main drawback is quick deactivation, which is mainly due to coking by carbon deposition. Coke formation is caused mainly by methane decomposition (Eq. 4), which is an endothermic reaction and favoured at high temperatures and lower pressures, and carbon

monoxide disproportionation (Eq. 5), which is an exothermic reaction and favoured at lower temperatures and higher pressures [55].

$$CH_{4\,(g)} \rightarrow C_{(s)} + 2H_{2\,(g)} \qquad \Delta H^{o}_{298\,K} = 75.2 KJmol^{-1} \qquad (4)$$

$$2CO_{\,(g)} \rightarrow CO_{2\,(g)} + C_{(s)} \qquad \Delta H^{o}_{298\,K} = -173.0 KJmol^{-1} \qquad (5)$$

It is however important to design a Ni-based catalyst with prolong activity and stability for high efficient conversion of the CO_2 and CH_4. Surface morphology such as size and acidity/basicity of Nickel supported catalyst are found to affect coking. Nickel particle size below 6nm has reported to show no carbon deposition and large Ni-clusters, which favour the formation of core/shell, promote carbon deposition [56].

The acidity/basicity of support also plays a crucial role on catalyst performance in DRM reaction. The catalyst support with strong basic characteristics generally enhances reactant CO_2 adsorption, hence facilitating gasification of carbonaceous deposits, whereas strong acidity sites promote the growth of carbonaceous deposits [57].

Thus, oxides with high oxygen exchange capacity and mobility have been reported in different literatures to be good candidates as supports that may mitigate carbon deposition and activate CO_2 through surface oxygen vacancies formed in presence of a reducing atmosphere for the DRM reaction. The use of ZrO_2 or CeO_2 can result in attractive process benefits owing to its redox behavior, surface acidity, reducibility and high thermal stability, When compared to irreducible oxides, such as Al_2O_3 or SiO_2 [58, 59].

Pt/ZrO_2 with or without promoter have been extensively studied in the literatures and confirmed to show better stability and catalytic activity, due to resistance to coking [60].

The stability and activity of Ni-based catalysts has been improved by the use of co-catalysts and the use of different promoters such as (K, Li, Ca, Na, Ce, La and Sr) [61].

Igor Luisetto et al. recently in their studies compared the catalytic activity of bimetallic Ni-Co with individual Ni or Co supported on Ceria (CeO_2) and found out that bimetallic catalyst showed higher conversion (50% at 600^oC and 97% at 800^oC) to methane than other two individual catalysts, probably due to the intrinsic nature of the Co-Ni alloy and not to a better dispersion of the active phase in smaller particles. Also stated in the same report that Cobalt-containing catalysts showed a stable operation during 20 h on stream, with a minor CH_4 conversion decrease of 0.5% in the case of Co/CeO_2 and 2% in the case of $Co\text{-}Ni/CeO_2$. Otherwise, Ni/CeO_2 showed the highest deactivation with a CH_4 conversion decrease of 8% [62].

Atiyeh R. and Mehran R. recently prepared different nickel loading on nanocrystalline calcium aluminate by co-precipitation using surfactant, and they observed that the support has high potential for methane dry reforming. Their results showed that high nickel loading of 15% has highest catalyst activity and affinity for carbon deposition, and 7% nickel loading showed highest stability with time on stream of 50 h than higher loading, due to high dispersion and specific surface area [63, 64].

Barroso-Quiroga, M.M. et al. reported nickel activity on different ceramic supports (Al_2O_3, CeO_2, La_2O_3, and ZrO_2), and found that ZrO_2 showed highest stable activity. In the same report, CeO_2 has relatively good activity but shows signs of deactivation after certain time during the reaction, and addition (0.5wt% Li and K) of modifiers improved the stability over 7h time on stream with no coke deposition but decrease in conversion compared to unmodified Ni/CeO_2 catalysts [61].

Incorporation of low amount of potassium (0.2wt%-K_2O) with nickel supported on alumina showed acceptable high activity (63% CH4 conversion) for constant 24h and very low coke deposition (< 30mgC/g cat.) for 6h TOS [65].

In general, type of the support and modifiers greatly affects the coking inclination. An effective way in preventing coke formation is the addition of alkali or alkaline earth oxides and lanthanides. On the other hand, the increase of Lewis basicity of the support enhances the ability of the catalyst to chemisorb CO_2, in the CO_2 reforming of methane and the adsorbed CO_2 reacts with C to form CO, resulting in the reduction of coke formation [63].

CHAPTER 3

METHODOLOGY

3.1 Materials and Reagents

β-SiC foam (60 PPI, 8 cm diameter cylinder) having BET surface area of 33 m^2/g was obtained from SiCAT Germany, and diced into suitable pieces, $Fe(NO_3)_3.9H_2O$, $Ni(NO_3)_2.6H_2O$, Tetra ethyl orthosilicate (TEOS), 1-propanol, 1-butanol, HNO_3, and CTAB are purchased from Sigma-Aldrich. All gases used are of high purity (H_2, C_2H_4, Ar, N_2, Air) 99.999% from Saudi industrial gas company (SIGAS).

3.2 Foam Modification.

Calcination of β-SiC foam was performed in high temperature electric furnace at 900^oC to create nanoscopic layer of silica. The temperature was ramped at 1^oC/min to 120^oC, held for 2 h to remove any presence moisture and other impurities, and then heat to 900^oC at 10^oC/min, and held for 3 h.

3.3 Synthesis of Mesoporous Silica by Evaporation Induced Self-assembly (EISA) and Wash Coating.

Evaporation induced self-assembly (EISA) was used in preparation of mesoporous silica by addition of 28.057 g of 1-propanol to 15.040 g of TEOS and stirred for 5 min, followed by 1.037 g of concentrated nitric acid (1M) and 3.980 g of De-ionized water, stirred for additional 60 min. Silica solution was obtained after addition of 14.105 g (1-

butanol). 3.947 g of CTAB and 8.816 g of De-ionized water previously stirred for 10 min was added to silica solution prepared and allowed to age for 2 hr [66].

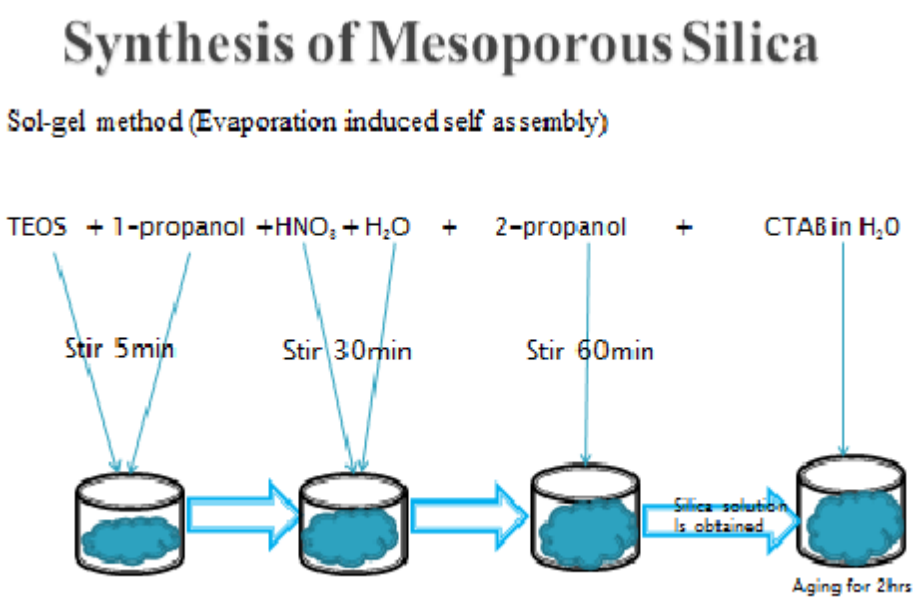

Fig.3.1: Schematic representation of evaporation induced self-assembly of mesoporous silica.

3-D β-SiC foam previously calcinated at 900^{o}C for 4 hr. was immersed in a self-assembly mesoporous silica solution by wash coating and dried at 105^{o}C to serve as interfacial oxide, which provide an anchorage site for active phase and help to increase the surface area of catalyst supports.

3.4 Catalyst Preparation:

Iron Nitrate Fe $(NO_3)_3.9H_2O$ and Nickel Nitrate Ni $(NO_3)_2.6H_2O$ are used as active phase precursors. Ca. 5wt%/ g of silicon-carbide foam loading of both Fe and Ni were deposited on to the support material using wet incipient wet impregnation (IWI) method. The impregnated samples are dried under fumehood overnight by air evaporation, followed by oven drying and calcination at 378 K and 823 K respectively.

3.5 CNSs growth

CNSs of different diameters were successfully grown by thermal catalytic chemical vapor deposition (T-CCVD) method using first-Nano CVD (Easytube 2000 - 64" length, 30" width, 60" height, 900 to 1300 lbs.) with 3" Quartz Reaction Chamber. After initialization of equipment (Pneumatic system, under Air), the furnace was heated between 973-1173 K under the flow of hydrogen gas (100 ml/min) to reduce oxide of iron and nickel to metal as growth catalyst. Finally, the CNF growth was carried out for 30min between 973-1173 K under constant flowing of ethylene and Hydrogen gas (50 ml/100 ml). Nitrogen and argon were used as carrier gas and zero-air for keeping reactor under pneumatic system.

Fig.3.2: 1st-nano CVD-reactor for catalytic growth of nanostructures.

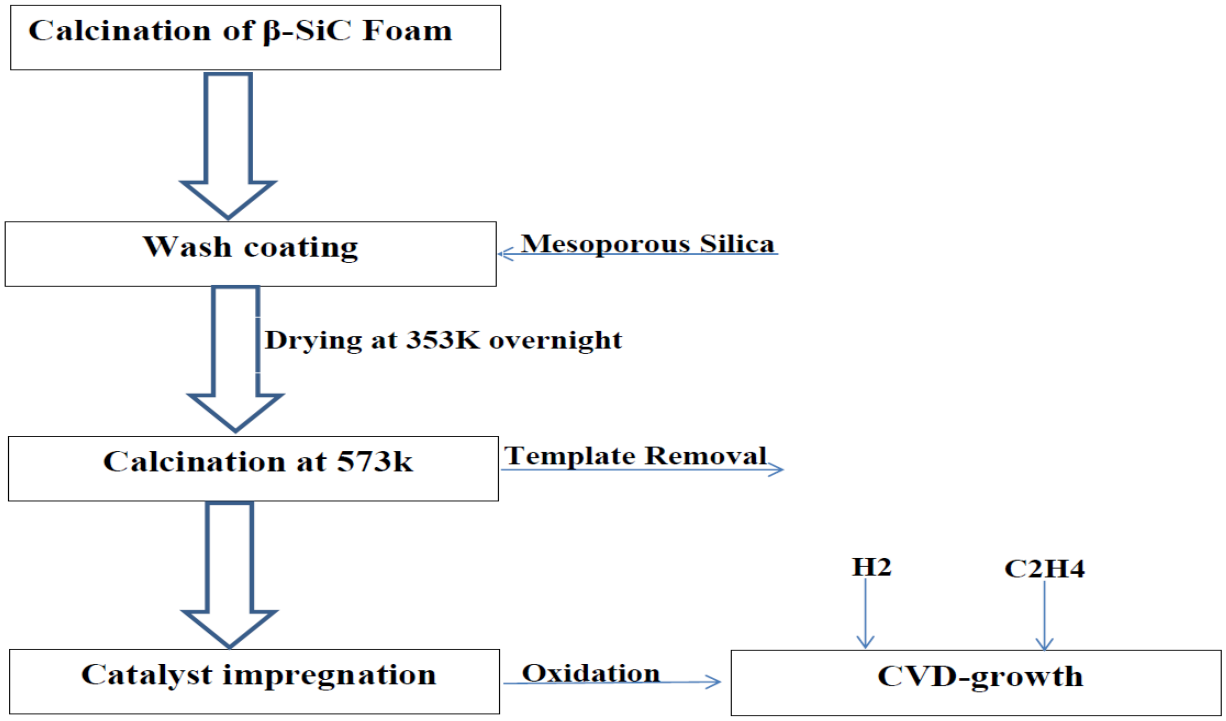

Fig.3.3: Schematic representation of CNSs growth on SiC-foam with mesoporous silica.

3.6 Carbon Nanofibers Functionalization.

The as-synthesized CNFs grown on 3-D SiC-foam support at 700^{o}C with nickel as growth catalyst was functionalized in acidic medium of HNO_3 to create hydrophilicity on the inert support. CNFs was soaked in 5 M nitric acid for 24 h, and then washed until neutral pH is achieved. The sample was dried at 80^{o}C overnight before active phase impregnation [67].

3.7 Structured Catalyst Preparation:

The acid functionalized carbon nanofibres were further impregnated with nickel precursor (Ni) using impregnation method described in (section 3.4) to prepare series of loading mass concentration (5wt %, 10wt %) for CNFs and bare SiC-foam as shown in Table 3.1.

Potassium Nitrate precursor was used to introduce K-promoter using successive impregnation method in the case of 5Ni-1K/CNF-SiC and 5Ni-2K/CNF-SiC, by dissolving in de-ionized H_2O, followed by impregnation of the acid- functionalized CNFs/SiC. After drying under fumehood, the catalyst was oxidized at 500^{o}C to K_2O and Nickel was introduced by incipient impregnation method. Co-impregnation was used for 10Ni-1K/CNF-SiC by wet incipient impregnation of potassium and nickel nitrate onto CNFs/SiC according to the method earlier described.

Table 3.1 Catalysts metal loading concentration and method of preparation for dry reforming of methane.

Cat-ID	Method of impregnation	Metal Loading
5Ni/CNF-SiC	IWI-single step	5wt%-Ni
10Ni/CNF-SiC	IWI-single step	10wt%-Ni
5Ni/SiC	IWI-single step	5wt%-Ni
5Ni-1K/CNF-SiC	Successive IWI	5wt%-Ni, 1wt%-K_2O
5Ni-2K/CNF-SiC	Successive IWI	5wt%-Ni, 2wt%-K_2O
10Ni-1K/CNF-SiC	Co-impregnation IWI	10wt%-Ni, 1wt%-K_2O

3.8 Methane Dry Reforming Evaluation

Dry reforming of methane was performed in a self-assembly fixed tubular reactor with column of 30 cm length and 2.5 cm diameter under atmospheric condition. As-synthesized Ni-structured catalyst was reduced in-situ prior to reforming reaction at 400^{o}C with heating rate of 10^{o}C/min and held for 2 h, under the flow of hydrogen gas with a flow rate of 100 ml/min. CH_4 and CO_2 gaseous feedstock were used in (1:1) according to stoichiometric reaction, with a total flow rate of 50 ml/min resulting in GHSV of 3000 ml/h gcat. The catalytic testing was done at temperature of 800^{o}C to study the activity of the catalyst and conversion of both feedstocks. The gaseous products (CO, H_2, CO_2 and CH_4) were detected and quantified in-situ with Bruker gas chromatograph, GC-450 using flame ionization and thermal conductivity detector. The following parameters were calculated and used to evaluate catalytic activity;

CH_4 conversion: $X_{CH4} = (F_{CH4,\ in}-F_{CH4,\ out})/F_{CH4,\ in}$

CO_2 conversion: $X_{CO2} = F_{CO2,\ in}-F_{CO2,\ out})/F_{CO2,\ in}$

H_2/CO ratio: $F_{H2,\ out}/F_{CO,\ out}$

Where Fi represent the mass flow rate of i-species.

Fig.3.4: Image of assembled reactor for dry reforming of methane.

Fig.3.5: Image of Bruker GC-450 for qualitative analysis of dry reforming reaction products.

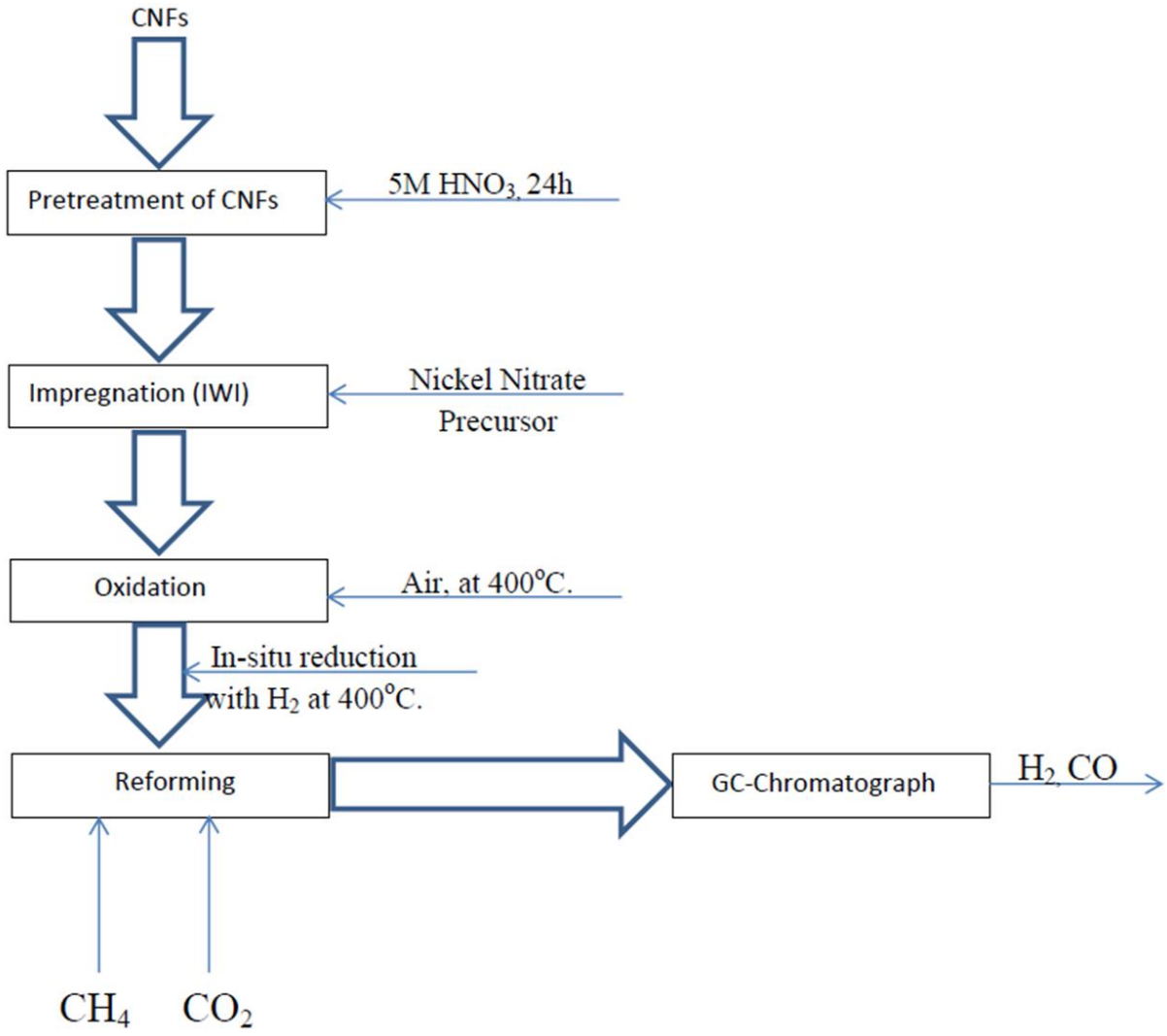

Fig.3.6: Schematic Representation of Dry Reforming of Methane Methodology using CNFs as Structured Catalyst.

3.9 Characterization Techniques for 3-D SiC Foam Support and Carbon Nanostructures

BET surface area of both 3-D solid support (SiC foam) and grown Carbon nanostructures on the support will be calculated on Tristar Micromeritics sorptometer (ASAP 2020 surface Area and Porosity Analyzer) using liquid nitrogen as an adsorbant at (-176^{o}C) temperature. Prior to BET surface area determination, the samples were degassed for 3 h at 250^{o}C to remove any presence of impurities.

TESCAN- LYRA 3 FESEM (manufactured in Czech Republic) was used to examine the morphology of SiC foam samples before and after Carbon nanofibers growth using SE and BSE mode with energy dispersive X-ray spectrometer detector for elemental analysis. TEM micrographs were taken by using FEI Company's TitanG2 60-300 ST operated at 300 keV energy, with a CCD Camera of model US1000 from Gatan, Inc., to examine the CNSs microstructure. It was equipped with Field-emission Gun and EDS detector from EDAX.

Raman spectroscopy technique (iHR320 with CCD detector, HORIBA, France) was employed at 532nm (300mW, green laser) to observe D and G-bands of CNSs and to evaluate the degree of graphitization of Carbon nanostructures grown by ratio of intensity of G-band to D-band (I_g/I_d). X-ray diffraction (XRD) using Cu anode (9 keV) at Kα =1.5405 (RIGAKU desktop minflex from Japan) was used to determine the crystallinity and degree of graphitization.

CHAPTER 4

RESULTS AND DISCUSSION

4.1 Effect of temperature on carbon nanostructures morphology

The growth temperature of carbon nanostructure is one of important parameters that determine its morphology. The SEM images of the as-synthesized CNSs are shown in Figure 4.1-4.8. The morphological images of as-synthesized CNSs grown on SiC-foam at different temperatures were observed by FESEM as a potential technique to confirm the uniformity, distribution, diameter, and shapes of the carbon nanostructures.

Carbon nanofibers of entangled form with average diameter of ca. 50 nm were observed between temperatures of 600^{o}C-700^{o}C using 5wt% of Fe and Ni per gram of SiC-foam support using (100 ml/min: 50 ml/min) flow rate of H_2 and C_2H_4 respectively. Entangled carbon nanofibers with high aspect ratio on carbon felt was grown using nickel as growth catalyst at 680^{o}C for catalytic applications Ledoux, M.-J. and C. Pham-Huu [45].

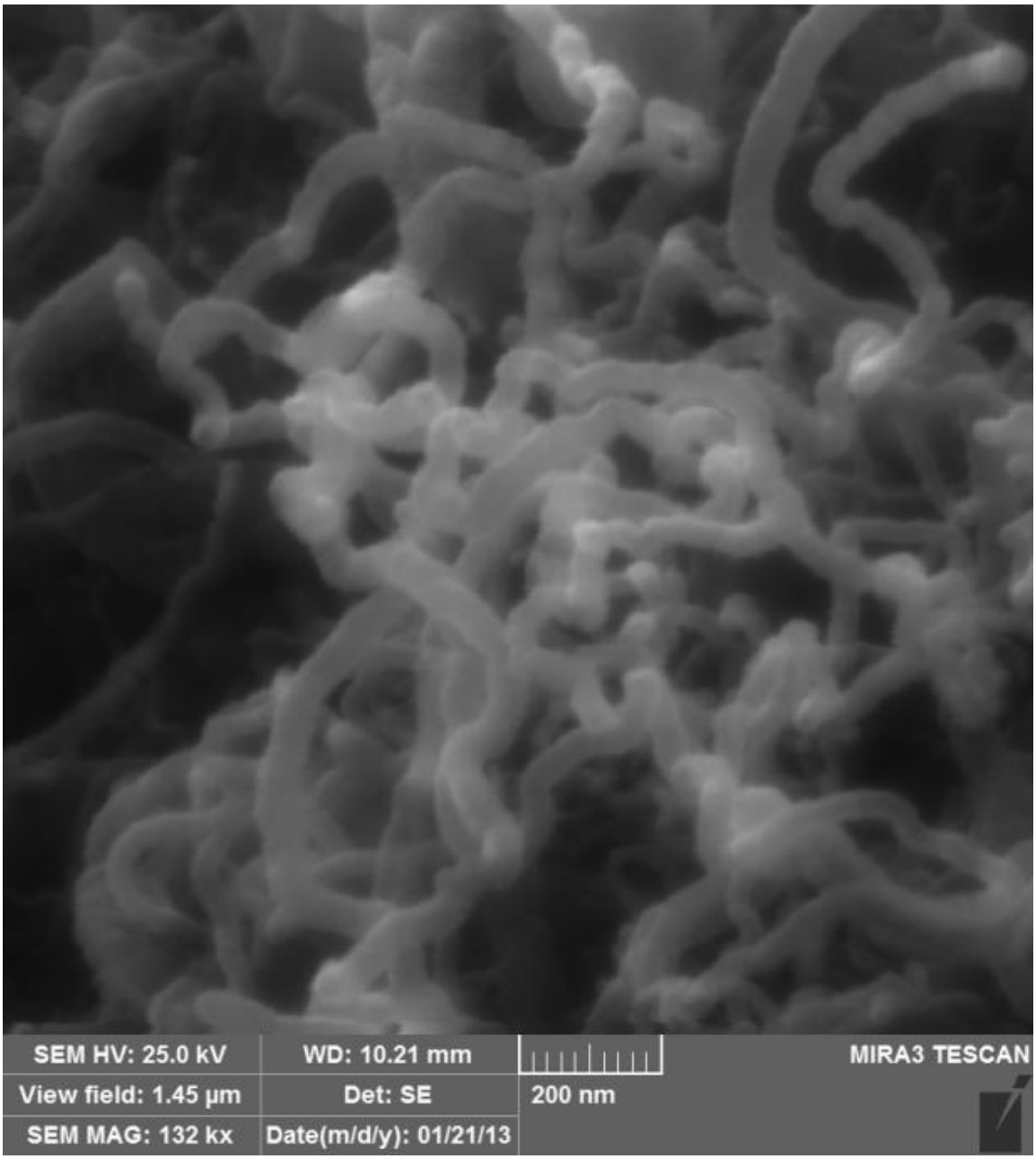

Fig. 4.1: Scanning electron micrograph image of CNF grown at 600^{o}C (100 ml/min H_2:50 ml/min C_2H_4) using 5wt%-Fe as active catalyst/g of SiC-foam support with average diameter of 50 nm.

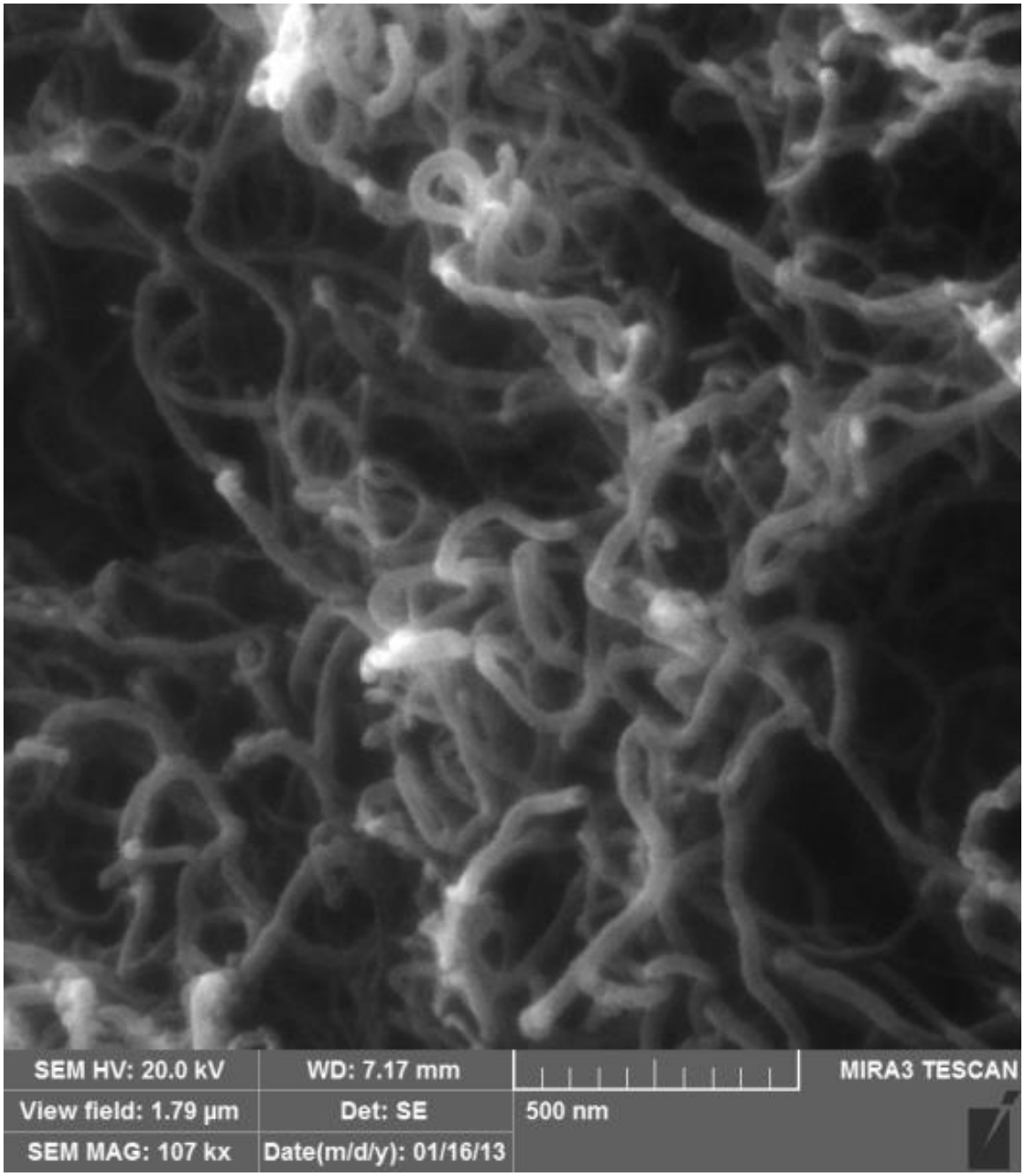

Fig. 4.2: Scanning electron micrograph image of CNF grown at 600^{o}C (100 ml/min H_2:50 ml/min C_2H_4) using 5wt%-Ni as active catalyst/g of SiC-foam support with average diameter of 50 nm.

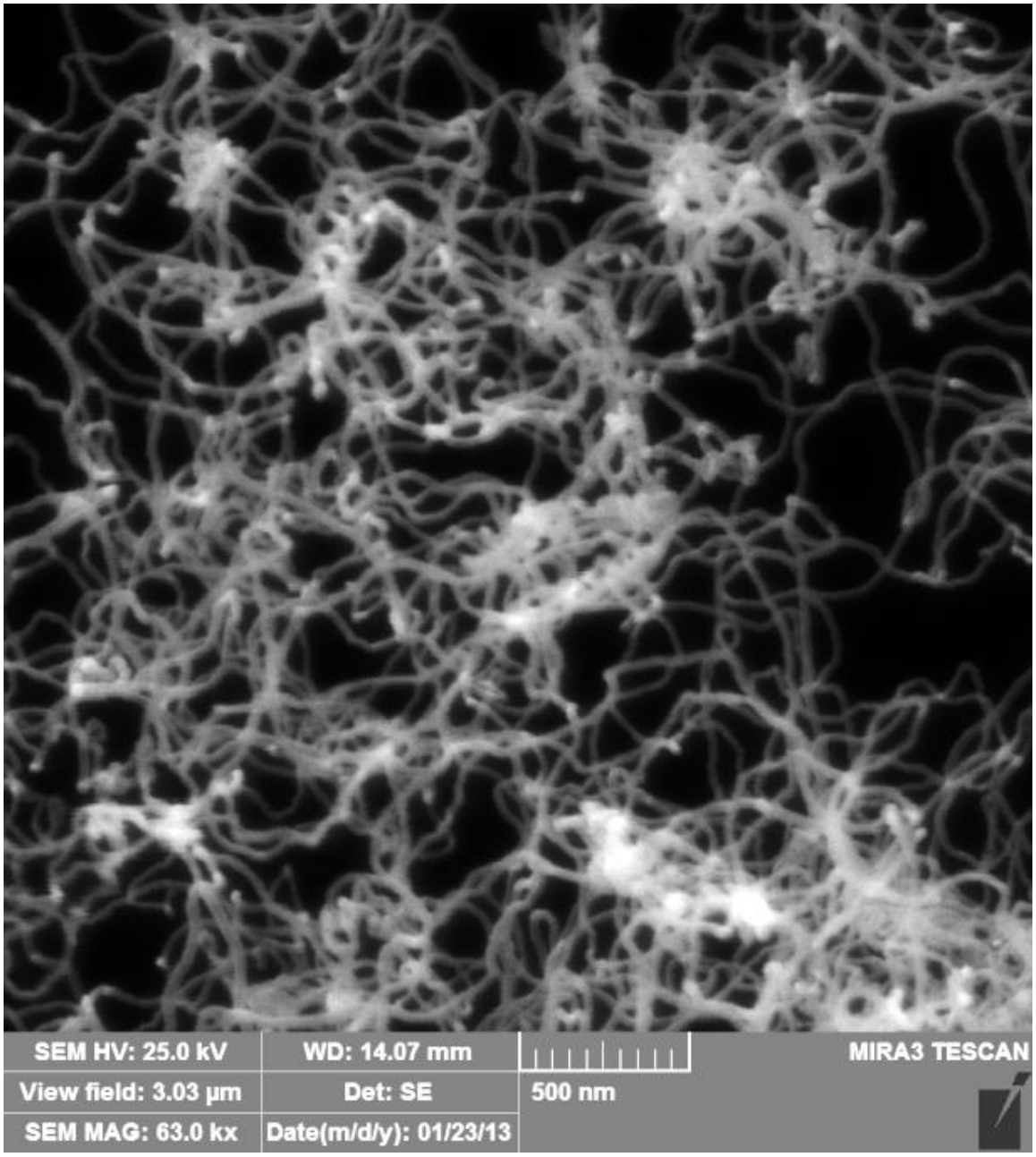

Fig. 4.3: Scanning electron micrograph image of CNF grown at 700^{o}C (100 ml/min H_2:50 ml/min C_2H_4) using 5wt%-Fe as active catalyst/g of SiC-foam support with average diameter of 50 nm.

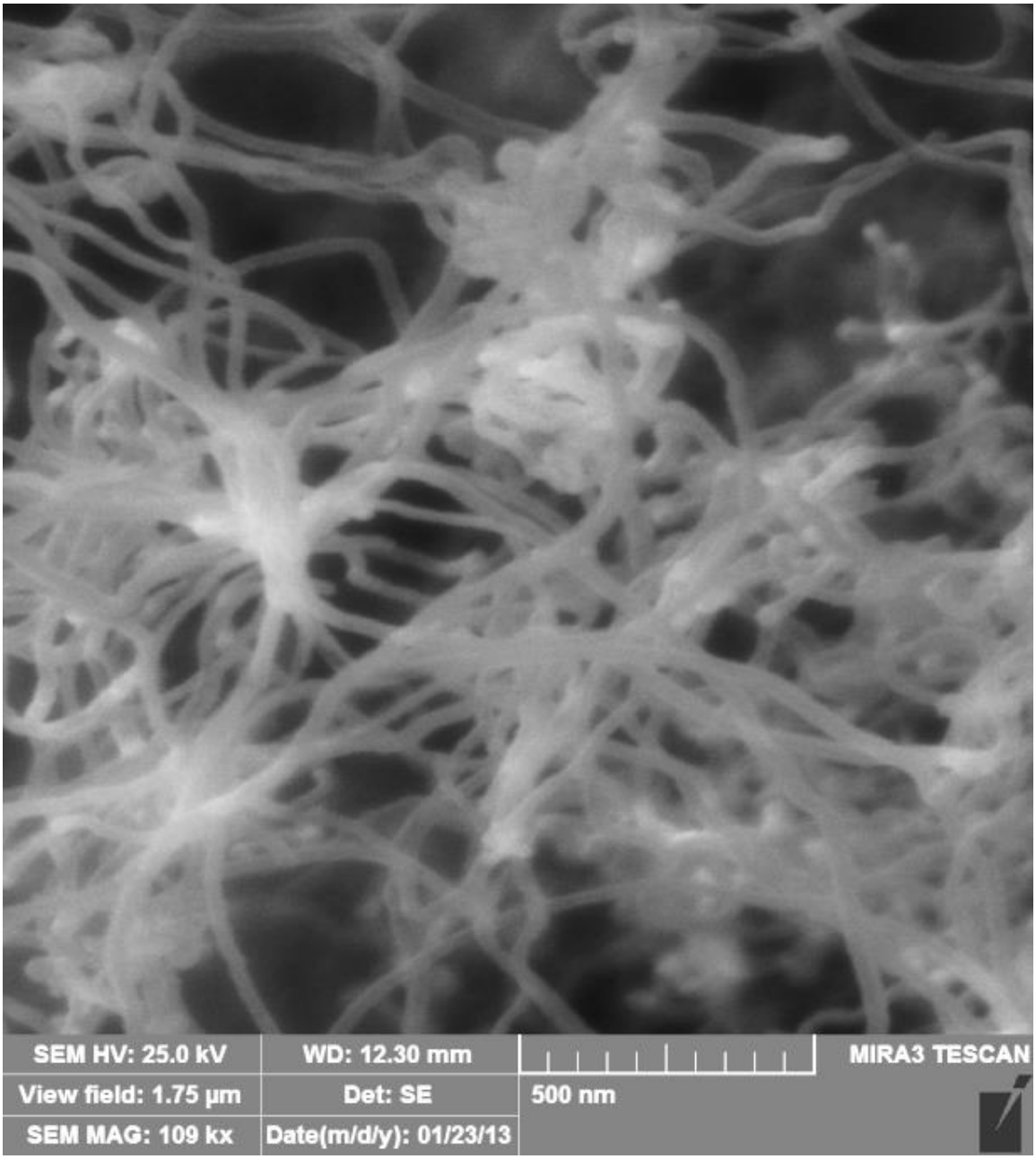

Fig. 4.4: Scanning electron micrograph image of CNF grown at 700^{o}C (100ml/min H_2:50ml/min C_2H_4) using 5wt%-Ni as active catalyst/g of SiC-foam support with average diameter of 50nm.

At 800^{o}C, there was an increase in average diameter of as-synthesized carbon nanofibers to 150nm for both Nickel and iron catalysts. The Ni-grown nanofibers were observed to be uniformly distributed on the SiC-foam support with the same entangled fiber of high aspect ratio, while there was partial loss of entangle in Fe-grown nanofibers. The observable results may be due to change in catalyst phase at high process temperature.

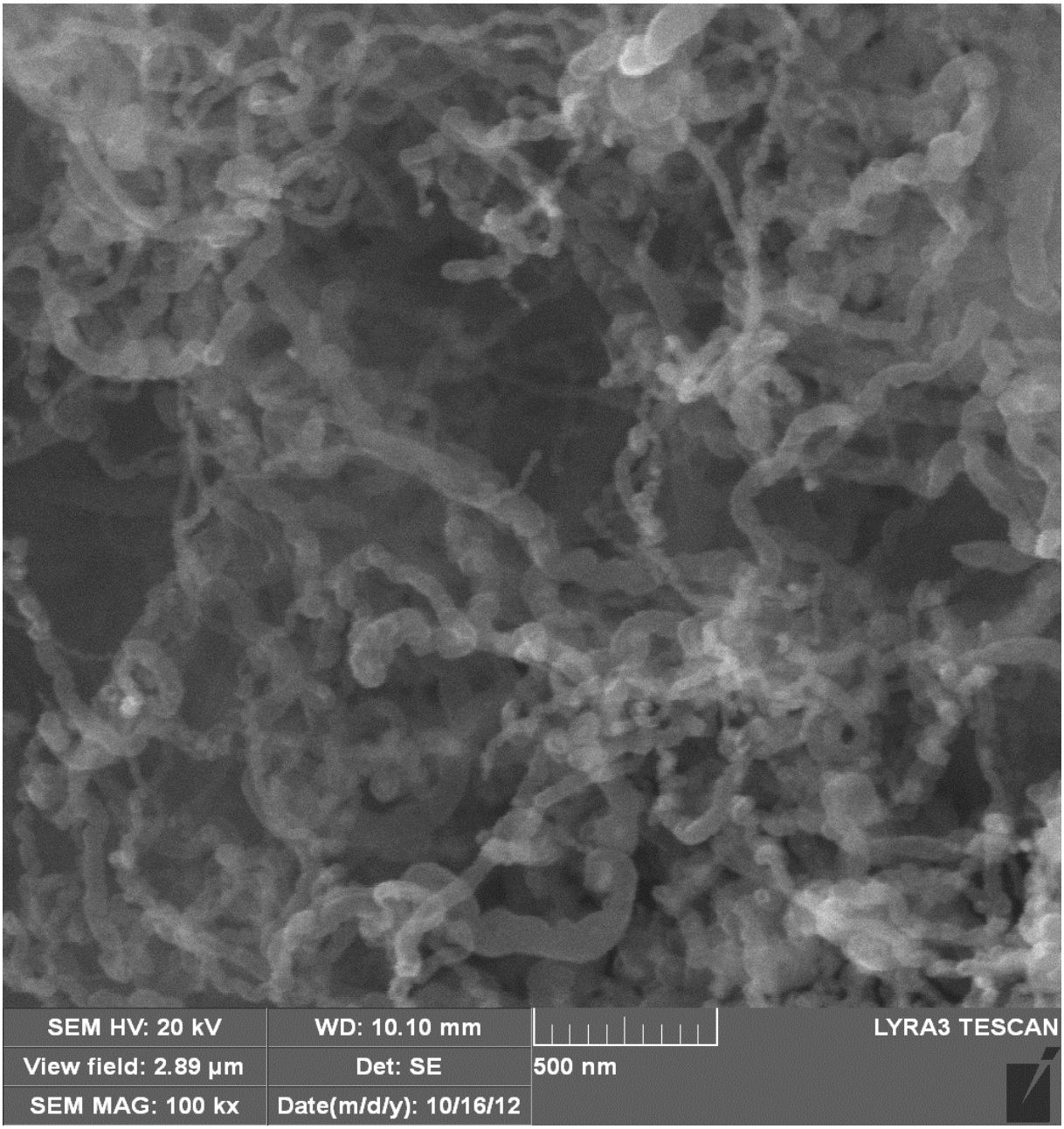

Fig. 4.5: Scanning electron micrograph image of CNF grown at 800^{o}C (100 ml/min H_2:50 ml/min C_2H_4) using 5wt%-Fe as active catalyst/g of SiC-foam support with average diameter of 100 nm.

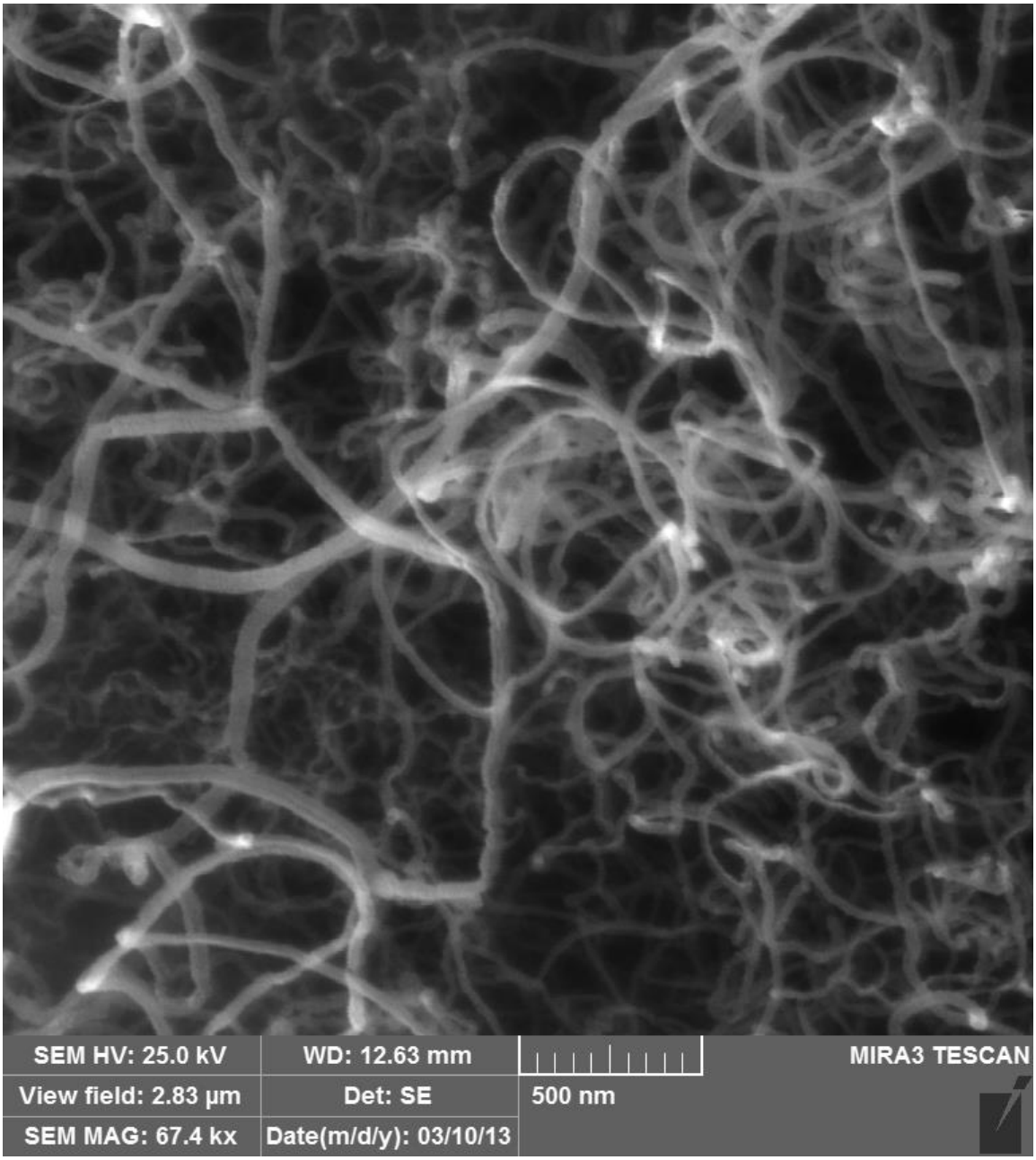

Fig. 4. 6: Scanning electron micrograph image of CNF grown at 800^{o}C (100 ml/min H_2:50 ml/min C_2H_4) using 5wt%-Ni as active catalyst/g of SiC-foam support with average diameter of 100 nm.

However, there was a morphological variation from carbon nanofibers to carbon nanobulbs at 900^{o}C with diameter of bulbs ranges from 150-250nm, with the same concentration of both Ni and Fe, keeping all other process parameters constant. The change in morphology is in agreement with what was obtained by Zhang, C. et al., at high temperature of 850^{o}C, where they synthesized hollow carbon nano-onions on magnesium oxide (MgO) powders for application in electrochemical hydrogen storage [68].

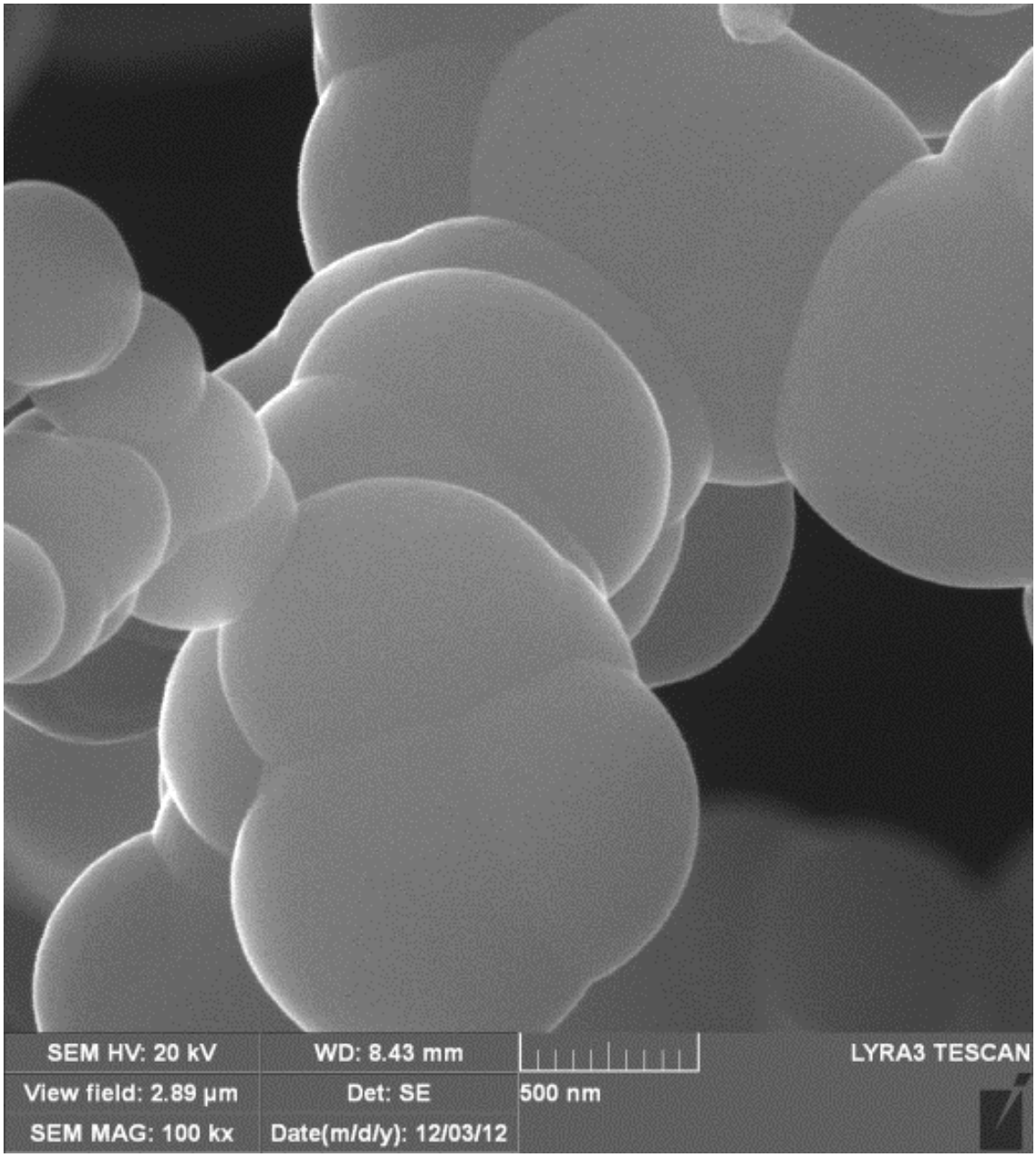

Fig. 4.7: Scanning electron micrograph image of CNF grown at 900^{o}C (100 ml/min H_2:50 ml/min C_2H_4) using 5wt%-Fe as active catalyst/g of SiC-foam support with average diameter of 250 nm.

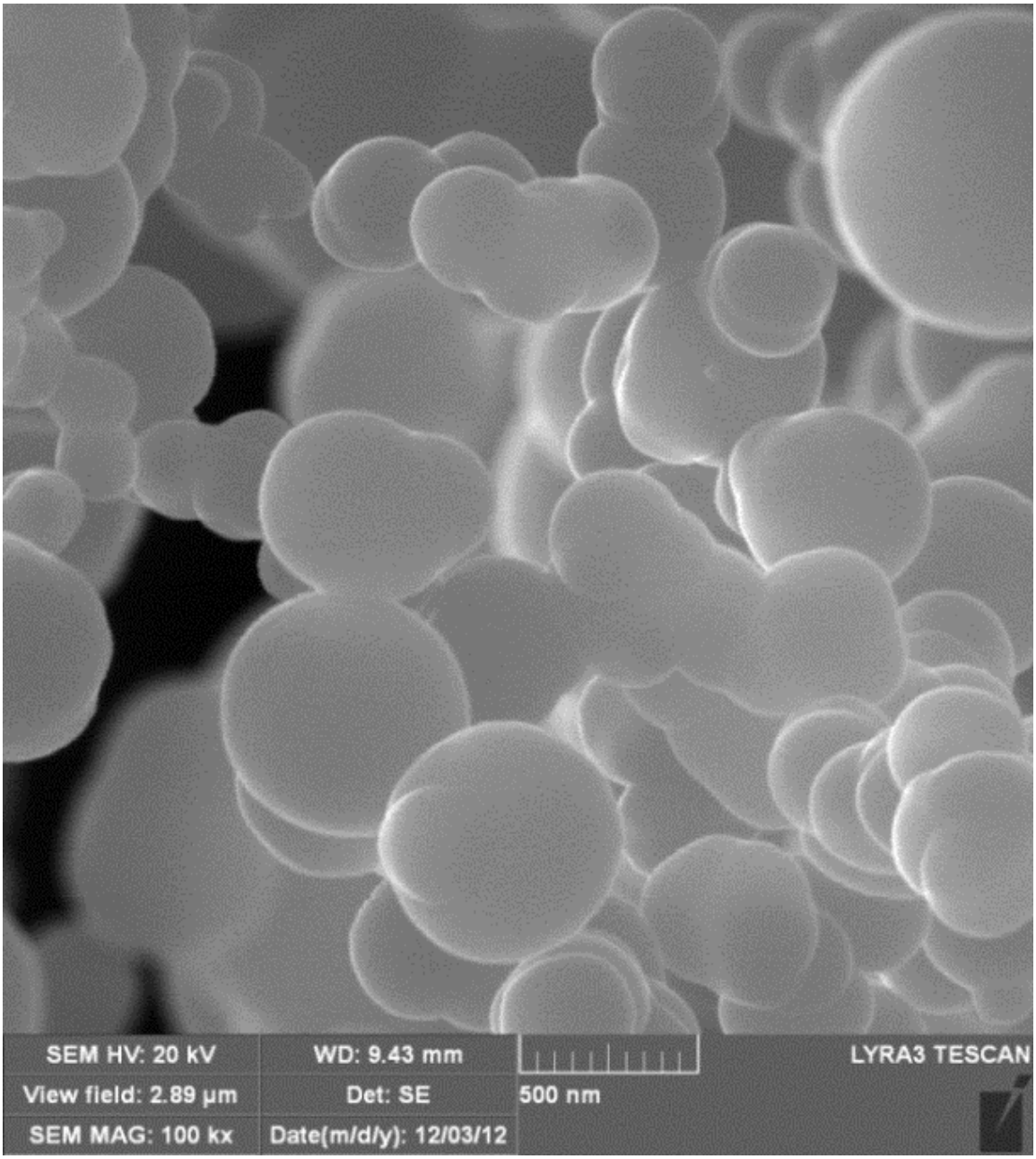

Fig. 4.8: Scanning electron micrograph image of CNF grown at 900^{o}C (100 ml/min H_2:50 ml/min C_2H_4) using 5wt%-Ni as active catalyst/g of SiC-foam support with average diameter of 250 nm.

Transmission electron microscope (TEM) was used to characterize the microstructure of carbon nano-materials with high resolution in order to obtain morphology, crystal structure and defects, crystal phases and composition, and magnetic microstructure. In addition, it is an important complimentary technique to scanning electron microscope (SEM) in evaluating and identifying the true nature of carbon nanostructures grown with or without support [69]. CNSs such as CNF and CNT (MWCNT) exhibit similar morphology and can only be distinguished by their observation through TEM, in which MWCNT is observed as 1D hollow tubes with both ends open or closed, and carbon nanofiber (stacked, platelet or cup) is 1D solid filled nanostructure [70, 71].

The TEM images of nanofibers were obtained at different magnifications to show the microstructure of as-grown CNFs at 700^{o}C for both Ni-CNFs and Fe-CNFs.

From fig 4.9, it was observed clearly that the nanofibers grown by CVD using iron-precursor as catalyst is 1D-solid filled fiber with very little traces of amorphous carbon along the growth axis of the fiber. In addition, the iron-particle of less than 50 nm diameter was observed within the fiber microstructure as shown in fig 4.9b, and this is an indication of no tip growth mechanism. The high-resolution micrograph in fig 4.9c reveals that the structure of the nanofiber is herringbone with 0.33 nm interplanar distances between two adjacent graphene planes.

The nanofibers microstructure obtained for Ni-grown CNFs was shown in fig 4.10a by low magnification TEM image. In confirmation of morphology observed by SEM, the TEM image reveals the fiber entangleness overlapping on one another and with little traces of amorphous carbon. The observed image show no tip growth of nanofibers, but

the solid inner core consist of nickel metal particle of 20 nm diameter. From fig 4.10c, the graphitic microstructure observed is herringbone, similar to the one obtained for Fe-CNFs in fig 4.9 and the interplanar distance is 0.335 nm [45, 70, 72].

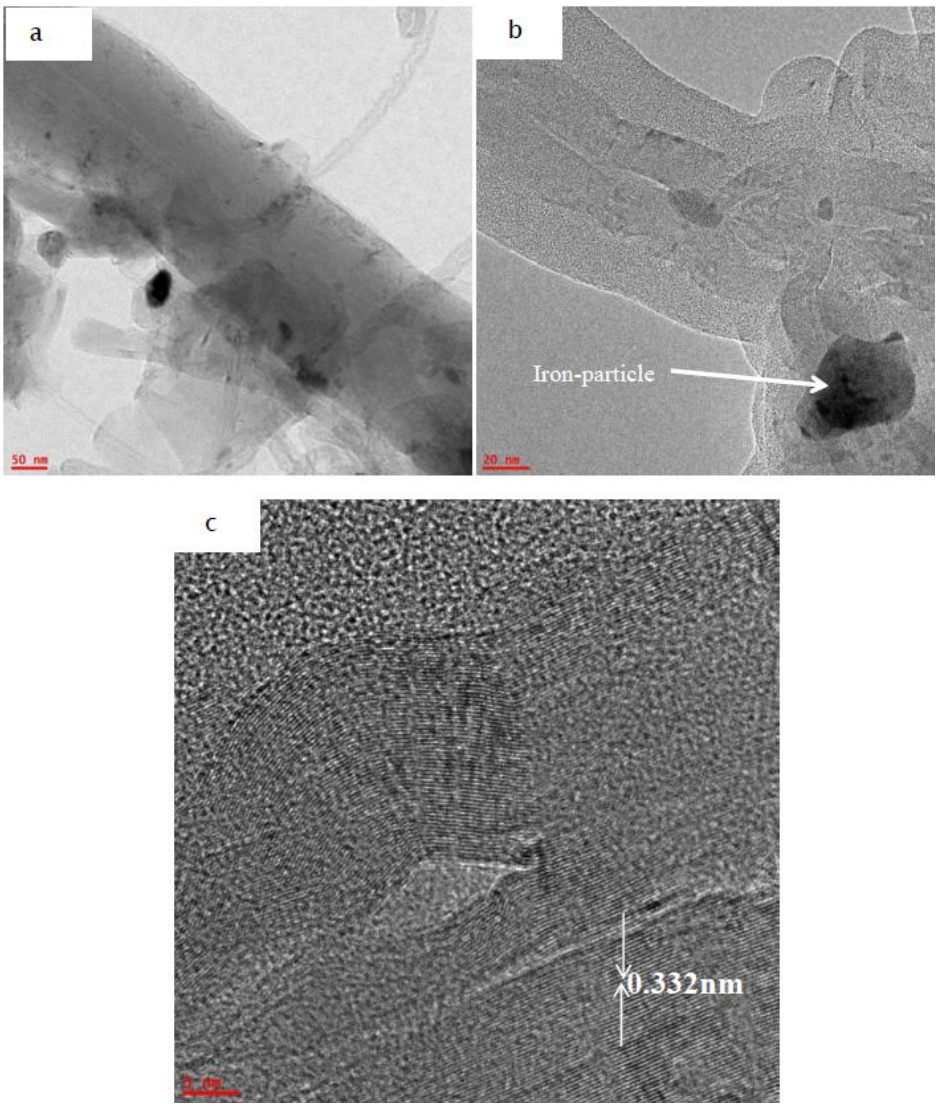

Fig. 4.9: TEM images at different magnifications of Carbon nanofibers grown on SiC-foam using iron-catalyst (Fe-CNF) at 700^{o}C on catalytic thermal chemical vapour deposition. (a) Low Magnification Image showing little presence of amorphous carbon along the growth axis of CNF (b) HR-TEM image of CNF showing the presence of Fe-particle along the growth of nanofiber (c) HR-TEM image of CNFs showing interplanar distance.

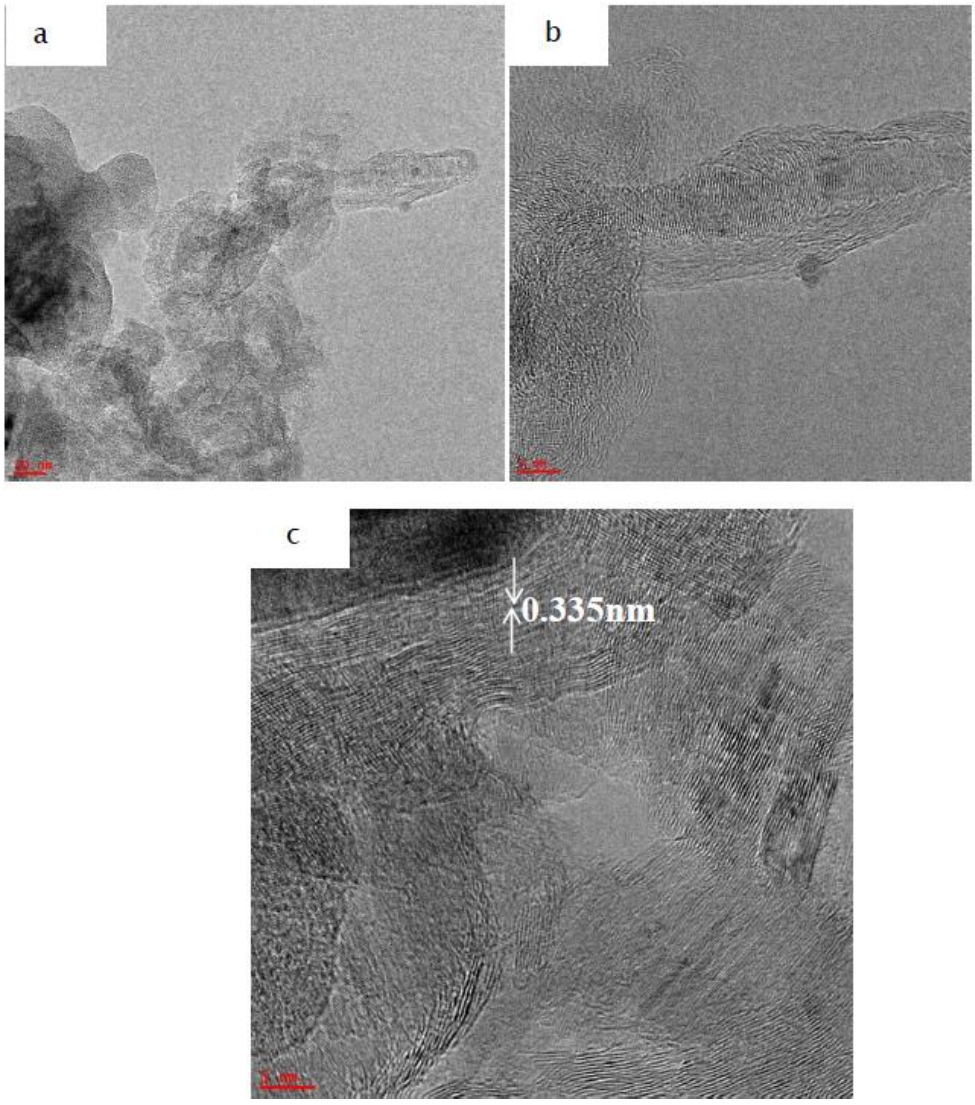

Fig. 4.10: TEM images at different magnifications of Carbon nanofibers grown on SiC-foam using nickel-catalyst (Ni-CNF) at 700^{o}C on catalytic thermal chemical vapour deposition. (a) Low Magnification Image showing little presence of amorphous carbon along the growth axis of CNF (b) HR-TEM image of CNF showing the presence of Fe-particle along the growth of nanofiber (c) HR-TEM image of CNFs showing interplanar distance.

4.2 Surface Area, Pore Size and Volume Measurement using N_2 gas Adsorption-Desorption

4.2.1 Effect of Interfacial Mesoporous Silica on Surface Area of SiC-Foam

Due to inert nature of the support material, interfacial mesoporous silica was employed to play a dual role in CNSs synthesis, (i) to provide anchorage site for catalytic active phase deposition, (ii) to increase the surface area of the support material.

Ordered mesoporous oxide film with a thickness of 100 to 300 nm was deposited via evaporation induced self-assembly (EISA) method. Surface area enhancement was achieved after deposition of mesoporous silica onto the support material from $33 m^2/g$ of as-received SiC-foam to 135 m^2/g, as obtained by the BET isotherm plot, (Table 1).

In addition to the surface area obtained by the BET method, pore size and volume were also obtained on the support (SiC-foam) and mesoporous silica (meso-SiO_2). Dependence of surface area on temperature was observed as shown in (table 1), when mesoporous silica deposited on support was calcinated at 300^oC, to remove organic template (cetyl trimethyl ammonium bromide, CTAB) used in the synthesis previously described in chapter 3. In general, specific surface areas of a mesoporous support decreases when subjected to high temperature for calcination. The BET surface area decreased from 115 m^2/g to 99 m^2/g.

4.2.2 Physiosorption Properties of SiC-Foam, Meso-Silica, and CNSs

Surface area, pore volume and pore size are important parameter in catalytic application, N_2 gas adsorption physiosorption was used to analyze the physical properties of as-received SiC foam after calcination, the mesoporous silica deposited on SiC- foam before

and after calcination and the as-synthesized carbon nanostructures at different growth temperatures.

In addition to surface area, pore volume and size distribution in catalysis are important to ensure mass and heat transfer to and from active surface. Smaller sizes are important in some catalytic reactions to limit unwanted reactions, and reaction by-products and feedstocks impurities could lead to loss of activity through pores blockage.

The observed trend in BET surface area at optimum growth temperature of 700^{o}C was; SiC/meso-silica/CNF >SiC/meso-SiO_2>SiC-Foam. In contrast, the trend of pore volumes and pore sizes are in descending order from support material (SiC-foam) to as-grown CNFs on the support, which is in good agreement with what has been reported in the literature [73]. The presence of very little micropores of about 2% in the bulk of as-received SiC-foam, confirms its suitability as catalyst and/or catalyst support and to bridge the gap of heat and mass transfer limitation encountered with conventional support in powdery form [74].

The as-received SiC-foam has lower surface area compared to mesoporous deposited SiC-foam without calcination (meso-SiO_2-WC) and with calcination (meso-SiO_2-C). However, the pore size and volume were reduced in both cases of Ni and Fe-grown, which was due to pore plugging during deposition of mesoporous silica on the support.

The as-grown CNFs at 700^{o}C for both Ni-CNF and Fe-CNF are characterized by high surface area (182m^2/g and 145m^2/g respectively) than the mesoporous deposited SiC-foam, with and without calcination due to smaller average diameter, uniform and

moderate distribution of the fibers on the solid support. The pore size and volume were reduced as expected due to smaller diameter of the CNFs grown, but still within the mesoporous.

From CNFs grown at 600^{o}C, the observed average diameter by SEM was 50 nm and the specific surface area of both as-grown Ni-CNF and Fe-CNF were lower compared to fibers at 700^{o}C. This reduction in surface area was attributed to increase in average diameter and excessive growth of CNFs on the support, while the pore size and volume were larger compared to CNFs grown at 700^{o}C.

Increase in average diameter, and excessive growth of CNFs at high temperatures (800-900^{o}C) caused loss of surface area than expected [46]. In addition to morphology variation from fibers to bulbs observed by SEM, the surface area of as-grown CNSs at 900^{o}C was below the surface area of as-received SiC-foam and the deposited mesoporous silica on the support in both cases of Ni and Fe-grown.

The as-synthesized carbon nanofibers were largely characterized by mesoporosity with high surface area at lower synthesis temperature while the high growth temperature that caused morphology variation also led to the loss of surface area and largely characterized by microporosity.

Clear distinction can be made from the carbon nanostructures grown from the use of nickel catalyst as active phase compared to iron. In all cases, nickel-grown nanostructures have high surface area in all range of temperatures.

Table 4.1 Summarizes surface area, pore volume and pore size of SiC-foam, SiC/meso-$SiO_{2,}$ at different conditions.

Sample Name	Growth-temp	$S_{BET}(m^2/g)$	$V_{TOTAL}(cm^3/g)$	t-$Plot_{\mu\text{-volume}}(cm^3/g)$	Pore size(nm)
SiC-Foam	-	34	0.1263	0.0027	14.9
SiC/meso-SiO_2-WC	-	135	0.1015	n.a	3.34
SiC/meso-SiO2-C	-	99	0.088	0.0015	3.54
SiC/meso-SiO_2/CNF-Fe-600	600	82	0.083	0.012	4.03
SiC/meso-SiO_2/CNF-Ni-600	600	131	0.13	0.017	3.88
SiC/meso-SiO_2/CNF-Fe-700	700	145	0.0698	0.046	1.92
SiC/meso-SiO_2/CNF-Ni-700	700	182	0.14	0.016	3.18
SiC/meso-SiO_2/CNF-Fe-800	800	35	0.073	0.0016	8.09
SiC/meso-SiO_2/CNF-Ni-800	800	53	0.071	n.a	5.27
SiC/meso-SiO_2/CNF-Fe-900	900	6	0.007	n.a	56.69
SiC/meso-SiO_2/CNF-Ni-900	900	15	0.029	0.0017	59.09

Excessive growth of carbon nanostructures weakens the support material and therefore the process parameter conditions must be accurately selected and controlled. The arrangement and distribution of nanostructures on the support should be relatively shallow to have optimum physical properties required to perform as structured catalyst or catalyst support. The CVD-growth temperature as shown in table 4.1 is responsible for increase and decrease in surface area of carbon nanostructures on the support [25].

4.3 Raman Spectroscopy

The Raman spectroscopy of carbon and carbon nanostructures is a well-established technique not only to give Raman vibrational information, but to also understanding structural and chemical changes needed to advance carbon nanomaterials for a given application, such as degree of graphitization and/or amorphotization, metallic or semiconductor type and diameters in case of (SWCNTs). First order Raman peaks usually appeared in the frequency range of 1000-2000 cm^{-1} [75], to give two strong peaks of carbon nanostructures known as D-band and G-band respectively. Figure 4.11 below is Raman spectra obtained for carbon nanostructures grown at 700^{o}C for both Ni and Fe.

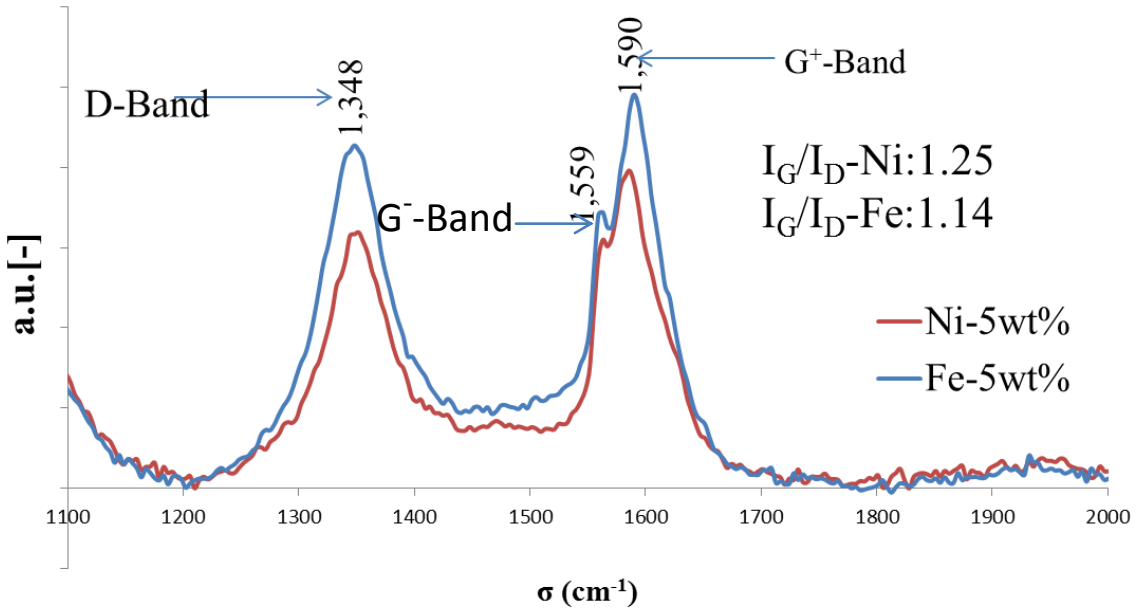

Fig.4.11: Raman spectra of Carbon nanofibers grown at 700°C.

The observed D-band (defect band) in graphitic carbon is generally due to impurities, pores, and symmetry defects in sp^2 carbon, while the G-band (graphitic band) is due to in-plane vibrational motion (E_{2g}) in carbon atoms. In many cases, the G-band used to split into G+ or G- due to vibrations along the nanostructure axis and circumference respectively.

The ratio of intensity of G-band to D-band (Ig/Id) is a measure or indication of degree of graphitization in carbon nanostructures. The higher the intensity of G-band relative to the D-band, the purer and crystalline is the CNFs, thus the higher the surface area, thermal conductivity, and the better the performance when applied as catalyst or catalyst support. The D-band was observed at 1348cm^{-1}, G^- and G^+ band were observed at 1559 cm^{-1} and 1590cm^{-1} respectively for CNFs grown at 700^oC. The observed intensity ratios (I_g/I_d) from Raman spectrum as a potential parameter to evaluate the quality of carbon nanostructures (CNSs) confirmed that the degree of graphitization is higher in nickel as a growth catalyst compared to iron. The observed trend in our experiment as shown in figures above confirmed that at optimum temperature of 700^oC the index of crystallinity is higher compared to others and decreases as temperature increases [40, 43, 76].

4.4 Crystallinity by XRD Pattern

The crystallinity of SiC-foam, active phase and the graphitic plane were observed by XRD patterns as shown in fig. 4.12 and 4.13. The As-received SiC-foam is a well crystalline support in beta-form with six different appreciable diffraction peaks. As observed from the figures, the corresponding peaks of SiC-foam at $2\Theta \approx 36^{o}$, 39^{o}, 42^{o}, 60^{o}, 72^{o}, and 75^{o}, with highest intensity peak observed at 36^{o}. Prior to XRD measurement of CNFs grown on the support, the active phase (Ni and Fe) deposited on the support with the aid of mesoporous silica did not show any diffraction peak different from that of support. In Ni-CNF (fig. 4.13), the Ni-crystallites with a face-centred cubic lattice of (111) and (200) observed at $2\Theta \approx 44^{o}$ and 58^{o} respectively, confirmed the presence and partly crystallization of Ni-catalyst in CNFs growth. However, the Fe-CNF shows different diffraction peaks (fig. 4.12) for iron particle phases, which coincided with that of SiC-foam support and the highest peak at $2\Theta \approx 36^{o}$. The graphitic plane corresponding to (002) phase is clearly observed at $2\Theta \approx 26^{o}$ in the case of Ni-CNF, while Fe-CNF is of low intensity. The degree of graphitization of CNFs are determined by the interlayer spacing (d_{002}), which are closer to that of ideal graphite (0.335 nm) in both cases of (Ni and Fe), which is 0.334 nm in Fe-CNF and 0.0335 nm in Ni-CNF. Nevertheless, the intensity observation from diffraction and TEM interspacing calculation shows that the degree of graphitization and/or crystallinity in Ni-CNF is higher compared to Fe-CNF and this is in perfect agreement with what has been obtained from ratio of intensities (I_g/I_d) of G-band and D-band by Raman analysis.

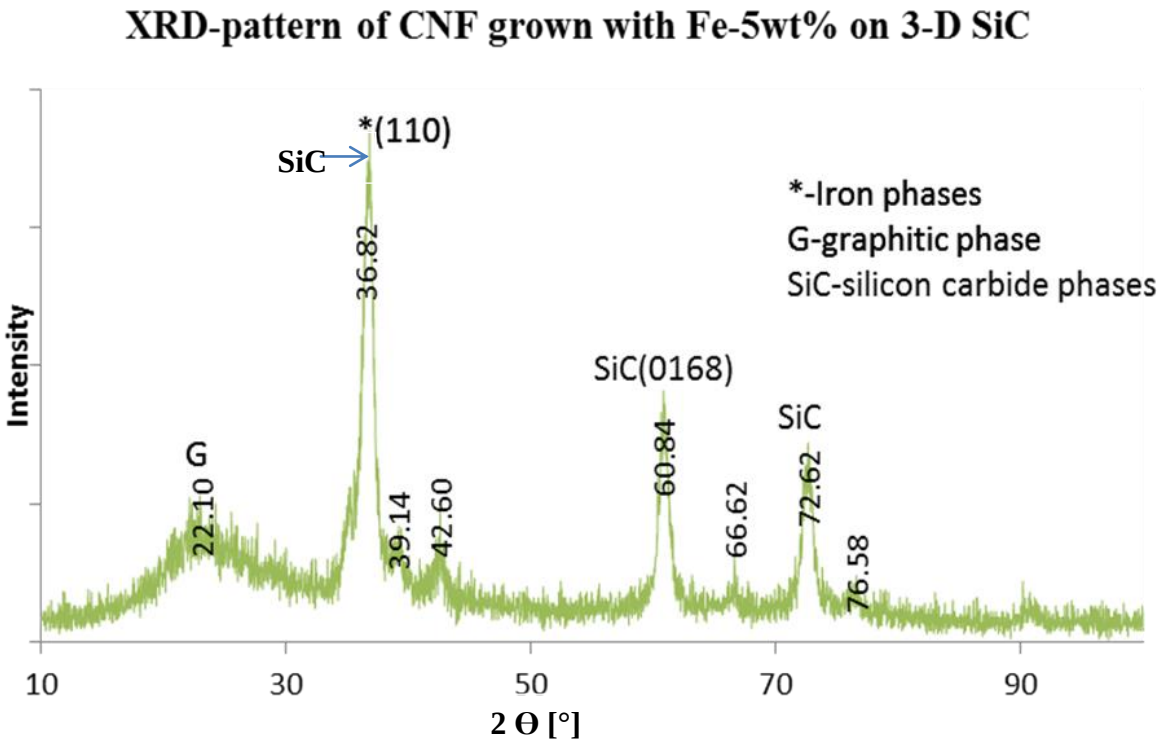

Fig. 4.12: XRD pattern of CNF grown on 3-D SiC foam support with Fe-5wt%/g of SiC-foam.

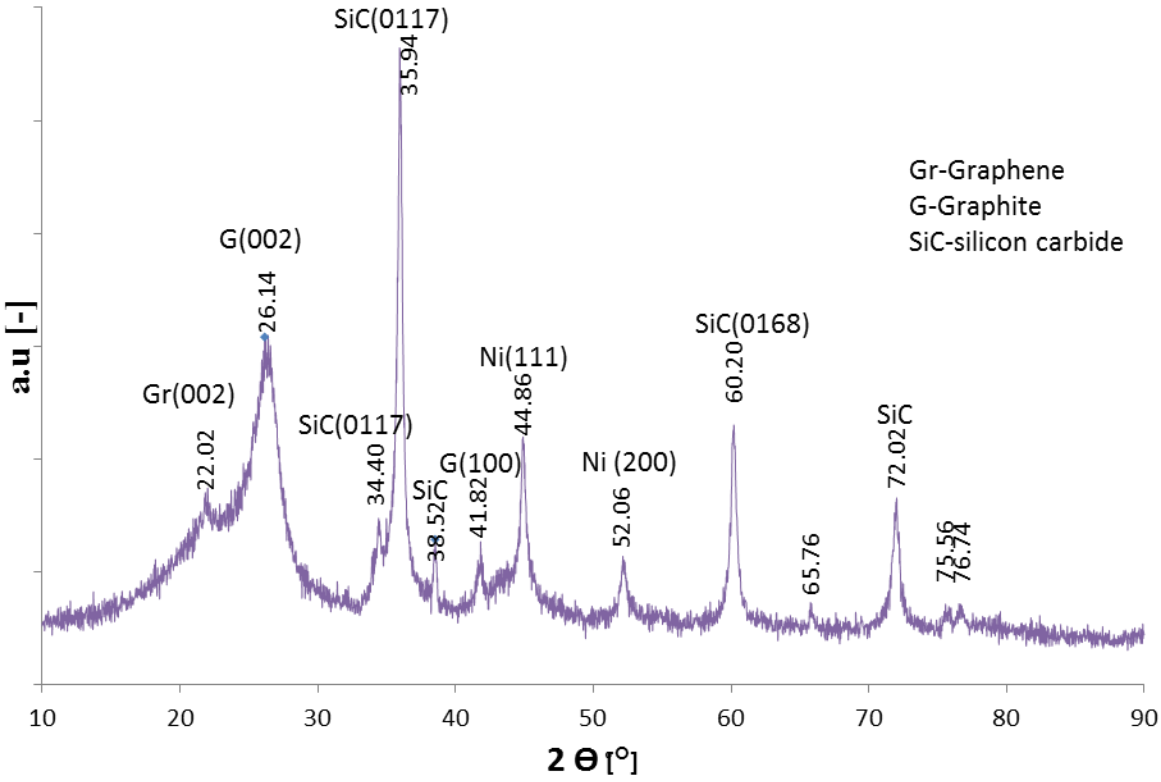

Fig. 4.13: XRD pattern of CNF grown on 3-D SiC foam support with Ni-5wt%/g of SiC-foam.

4.5 Dry Reforming of Methane Experimental Results and Discussion

4.5.1 Catalytic Activity and Stability of Different Catalysts for Dry Reforming

One of the main objectives of dry reforming is to consume two important greenhouse gases and convert them to useful products. Reforming products is either for production of syn-gas or to hydrogen. Syn-gas can be processed into methanol and other valuable oxygenated products, while demand for hydrogen for clean fuel source has also received tremendous attention.

Table 4.2 is a summary of different catalysts prepared and their potential to either produce syn-gas and/or hydrogen. In general, Nickel based catalyst has strong affinity to dissolve hydrocarbon source with selectivity towards hydrogen, but the use of promoter aid the production of syn-gas to methanol and other oxygenated products.

Table 4.2: Summarizes different catalyst conversion and selectivity ratio for dry reforming of methane at 800^{o}C (feedstock: CH_4:CO_2, 1:1).

Cat-ID	Average CH_4-Conversion (%)	Average CO_2-conversion (%)	Average H_2/CO ratio [-]
5Ni/CNF-SiC	62	46	2
10Ni/CNF-SiC	70	40	6
5Ni/SiC	32	28	5
5Ni-1K/CNF-SiC	60	50	1
5Ni-2K/CNF-SiC	45	52	1
10Ni-1K/CNF-SiC	70	75	4

4.5.2 Catalytic Activity of Carbon Nanofibers and Bare SiC-Foam over Nickel Catalyst.

The average conversion of CH_4 and CO_2 over 5Ni/CNF-SiC at reaction temperature of 800^oC with feedstock molar ratio of CH_4/CO_2= 1:1, as shown in Fig 4.14 was approximately 62 and 46% respectively. The catalytic operation was done over period of 15 h to observe the activity, the stability and H_2/CO yield of the catalyst against time on stream. It was observed that the catalyst was stable for over period of 8 h with H_2/CO ratio approximately two (2) Fig 4.15, which is suitable for syn-gas production and finally to methanol and oxygenated products. At higher time on stream, the ratio of H_2/CO was tending towards (3) and the conversion was dropped to 55% and 39% for CH_4 and CO_2 respectively, due to gradual deposition of filamentous carbon onto the active site of the catalyst.

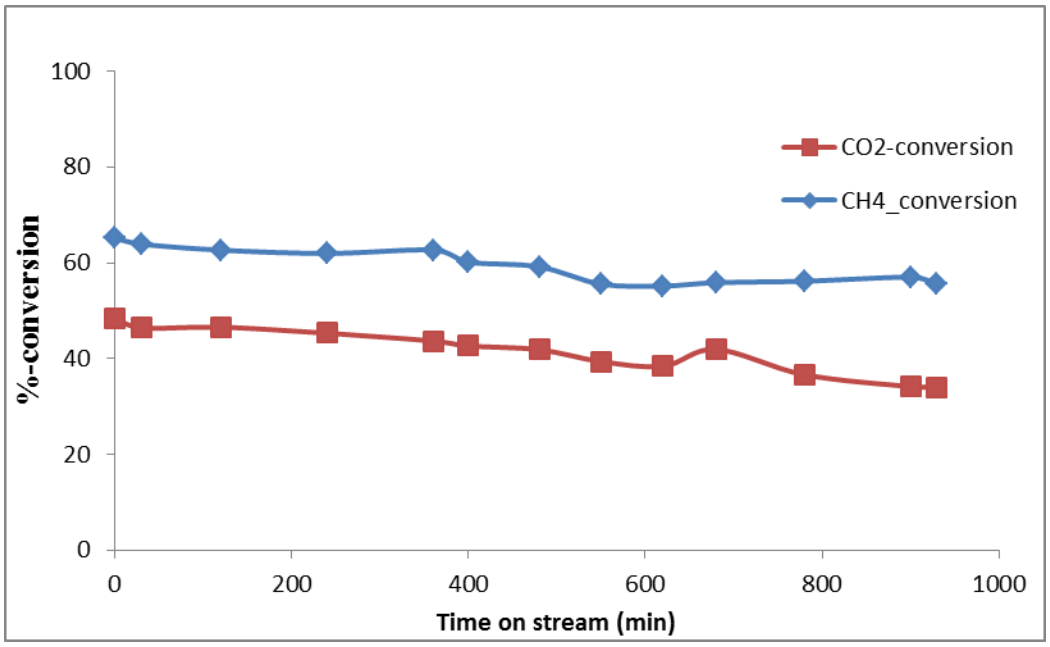

Fig. 4.14: CH_4 and CO_2 conversion with respect to time on stream over 5Ni/CNF-SiC catalyst at 800^oC for dry reforming (CH_4: CO_2= 1:1).

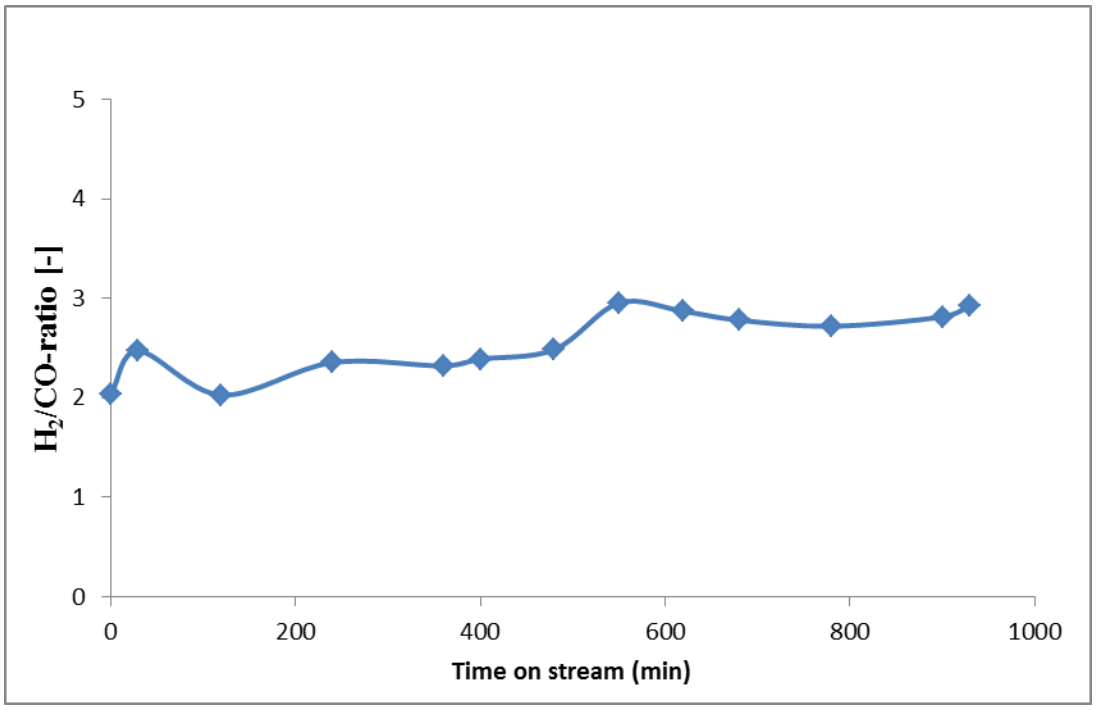

Fig. 4.15: H_2/CO ratio with respect to time on stream over 5Ni/CNF-SiC catalyst at 800^oC for dry reforming (CH_4: CO_2= 1:1).

On the other hand, the Nickel supported catalyst on bare SiC-foam (5Ni/SiC) with the same catalyst loading was used to compare its catalytic activity and selectivity with carbon nanofibers as shown in fig 4.16. It was observed that the conversion of both methane and carbondioxide was low, 32% and 26% respectively and the selectivity was towards hydrogen with H_2/CO ratio of approximate five (5) fig 4.17. The catalyst activity was shorter over the time stream. The reason might be due to poor dispersion of nickel active phase on the SiC-foam support, which in turn hindered its catalytic performance as compared to carbon nanostructure catalyst, with higher specific area and high dispersion, which gives relative better conversion, and stability.

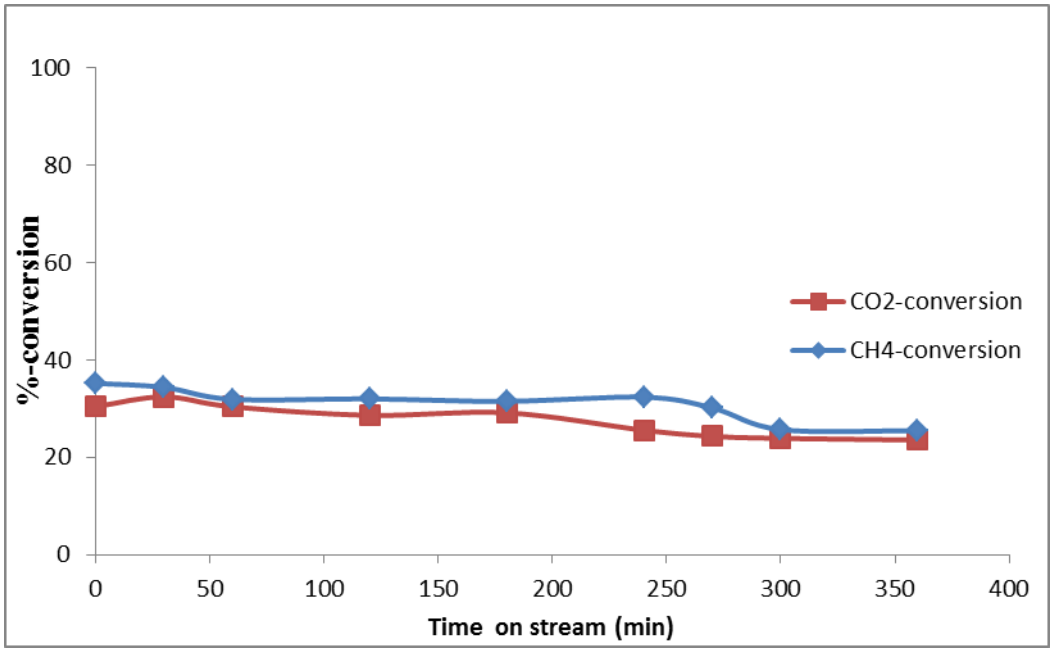

Fig. 4.16: CH_4 and CO_2 conversion with respect to time on stream over 5Ni/SiC catalyst at 800^oC for dry reforming (CH_4: CO_2= 1:1).

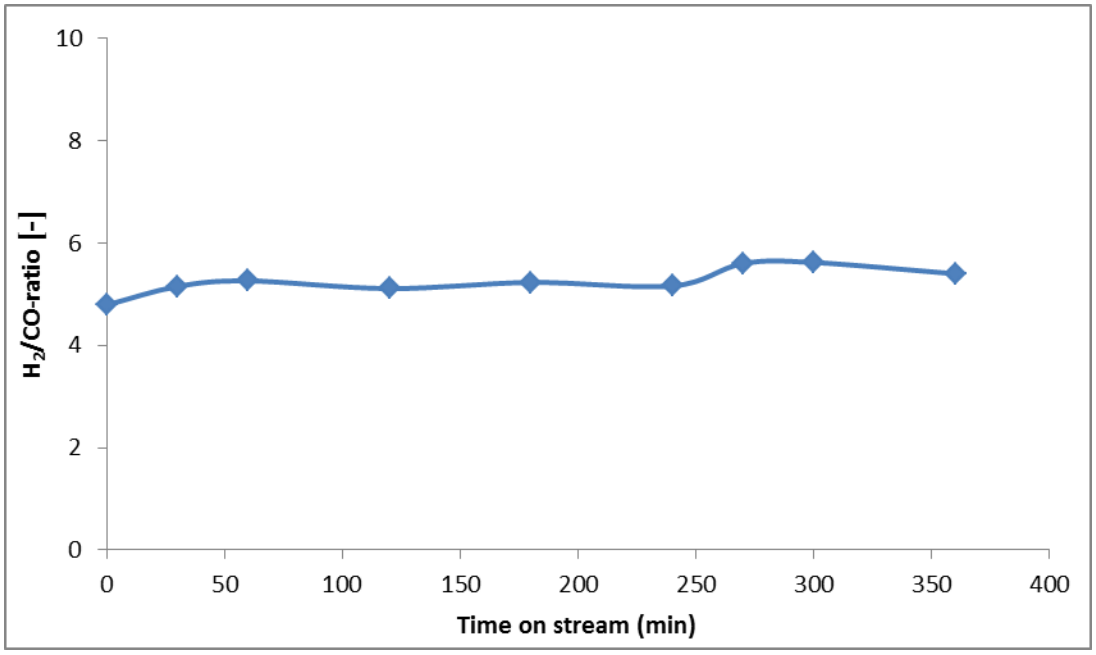

Fig. 4.17: H_2/CO ratio with respect to time on stream over 5Ni/SiC catalyst at 800^{o}C for dry reforming (CH_4: CO_2= 1:1).

4.5.3 Effect of Nickel Loading on Selectivity and Activity of Carbon Nano-structured Catalysts.

Fig 4.18 shows the CH_4 and CO_2 conversion and selectivity for 10Ni/CNF-SiC to compare the effect of nickel loading for dry reforming at the same reaction temperature. In contrast to 5Ni/CNF-SiC, the CH_4 conversion was high at thermodynamic equilibrium of 70%, but the CO_2 was 40%. The high methane conversion is associated with high nickel dispersion and more active stepped surface adsorbed on the nanostructure support than at 5wt% nickel loading. The observed low CO_2 conversion is caused mainly by high rate of filamentous carbon deposition on the support, and the inability of the support to gasify the deposited coke. In addition to high methane conversion, the H_2/CO ratio also increases with high nickel loading. The decrease in water shift gas reaction (WSGR) due to increase in nickel loading, also disfavor the conversion of CO_2. The trend of catalyst stability observed is better at lower nickel content, more than 10 h on stream before major decrease than at higher loading, because of high coke deposition explained above.

The carbon nanostructured catalyst in this case was highly selective towards hydrogen production than CO, and the ratio of the products was approximately six (6) which is not suitable for syn-gas and methanol synthesis.

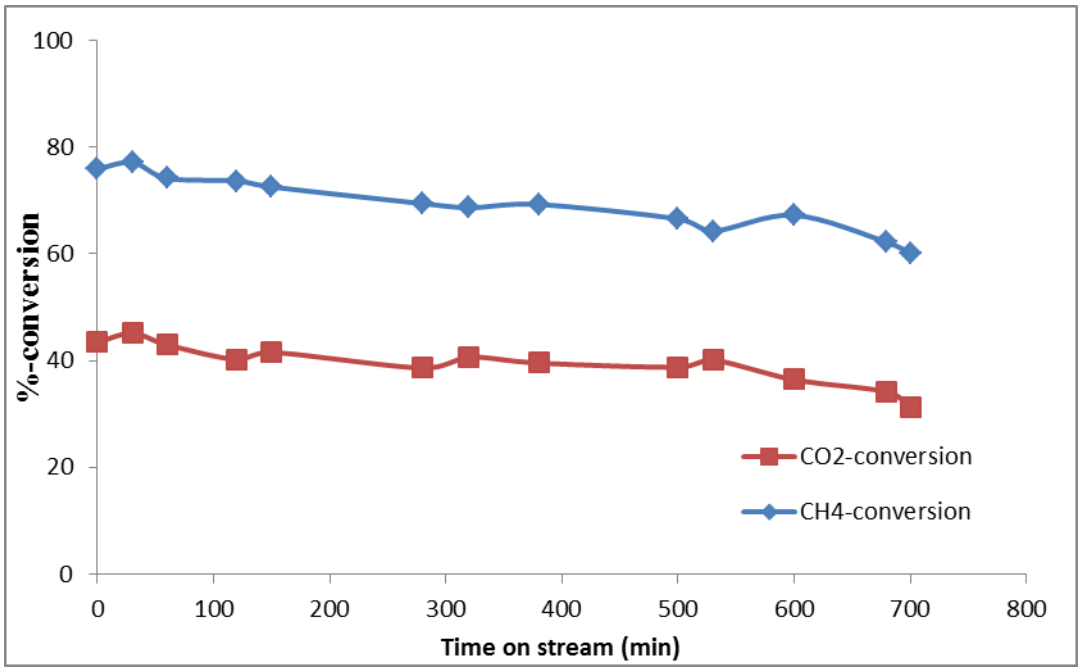

Fig. 4.18: CH_4 and CO_2 conversion with respect to time on stream over 10Ni/CNF-SiC catalyst at 800^oC for dry reforming (CH_4: CO_2= 1:1).

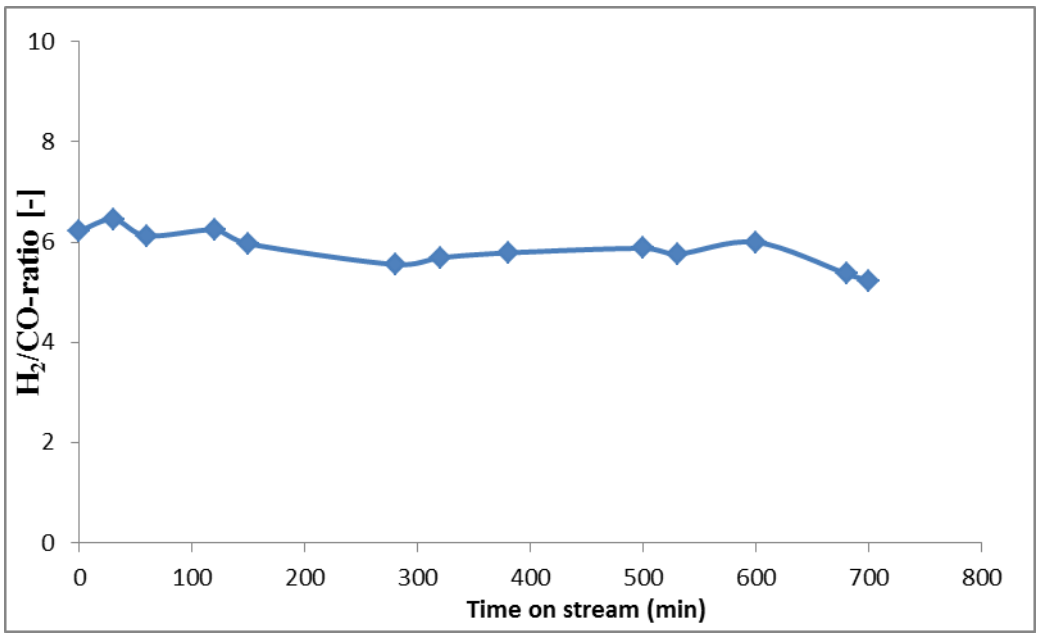

Fig. 4.19: H_2/CO ratio with respect to time on stream over 10Ni/CNF-SiC catalyst at 800^{o}C for dry reforming (CH_4: CO_2= 1:1).

4.5.4 Effect of Potassium-Promoter and Ni-Loading on Conversion and Selectivity on DRM

Incorporation of promoter (alkali and alkali earth metal) to structured catalyst increased its alkalinity, with better potential for CO_2 adsorption and activation, which accelerated the gasification of the surface carbons and retarded the formation of inactive carbon.

Potassium and other oxygen rich are good promoters for carbon gasification to provide localized oxygen at the surface, which hindered accumulation of adsorbed carbon on the surface and improved the catalytic activity and stability.

Series of K-promoter nickel supported carbon nanostructured catalyst as shown in (Table 4.2) were tested for dry reforming. In all cases of catalyst prepared, the CO_2 conversion was increased due to enhance rate of coke gasification, and decrease in methane conversion below the thermodynamic equilibrium conversion. The reason is associated with what has been reported in the literature from DFT investigation that active stepped phase of nickel is blocked by the presence of promoters caused by migration of potassium from the support to nickel phase, while the close-packed terraces and other unblocked active site will be used for reforming. The close-packed terraces are less active for methane reforming and coke formation [77, 78].

Fig 4.20 shows methane and carbondioxide conversion over 5Ni-1K/CNF-SiC at 800^{o}C to evaluate the effect of potassium promoter for reforming. The nickel loading is ca. 5wt% with 1wt% k_2O prepared by successive impregnation method. It was observed that CH_4 conversion was lower compared to 5Ni/CNF-SiC without addition of promoter and increase in the CO_2 conversion, which is due to blocking of some active site of nickel by potassium. The products selectivity ratio (H_2/CO) of this catalyst is close to unity for

almost 13 h on stream as shown in Fig 4.21. The result obtained in this case is a consequence of two effects of potassium-promoter previously discussed: the blockage of Ni active sites for methane decomposition and the enhancement of coke gasification, which is suitable for syn-gas, methanol and other oxygenated products [65, 79].

There was a decrease in selectivity ratio of H_2/CO below unity and as well conversion of methane after 13 h.

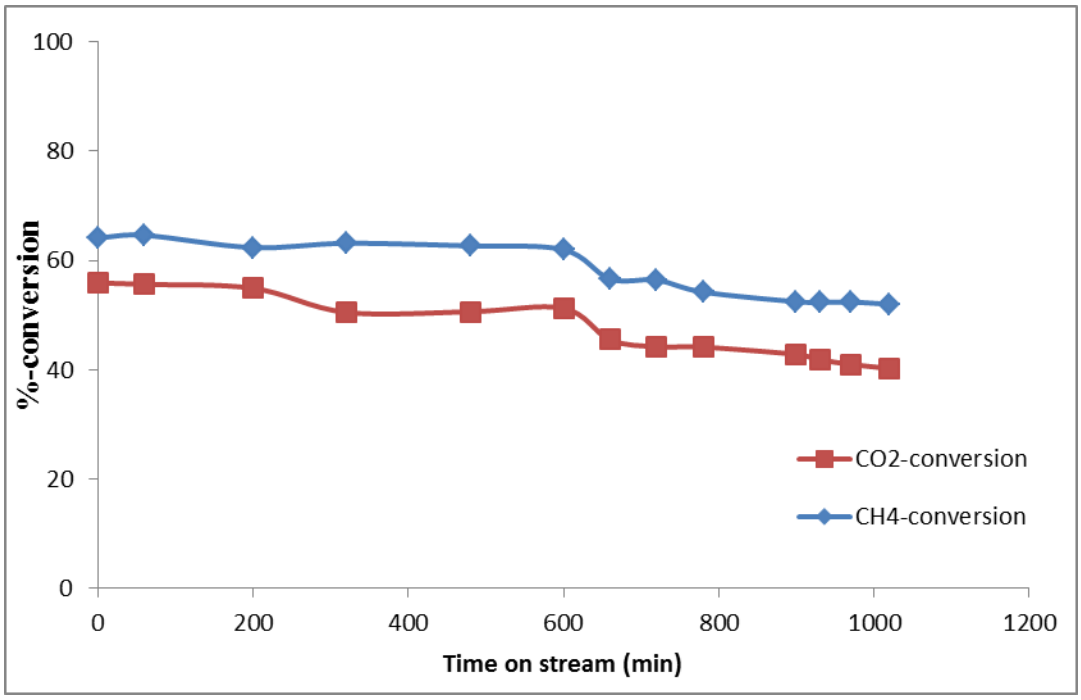

Fig. 4.20: CH_4 and CO_2 conversion with respect to time on stream over 5Ni-1K/CNF-SiC catalyst at 800^oC for dry reforming (CH_4: CO_2= 1:1).

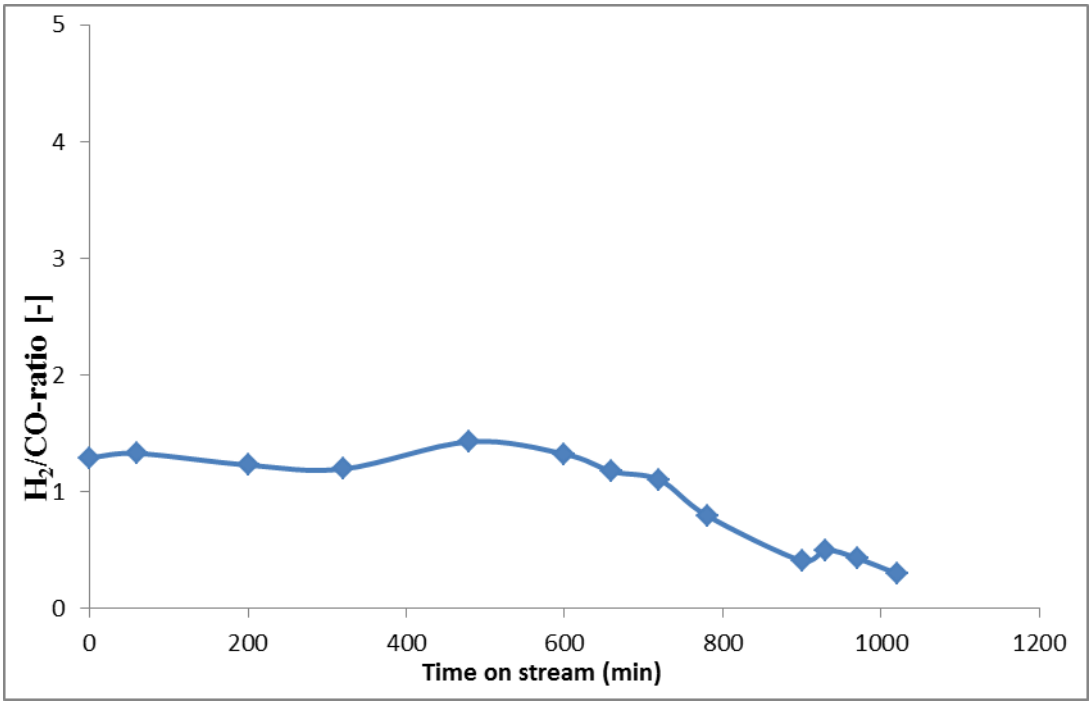

Fig. 4.21: H_2/CO ratio with respect to time on stream over 5Ni-1K/CNF-SiC catalyst at 800^{o}C (CH4: CO2= 1:1).

In addition, potassium loading content on nanostructured catalyst increased from 1-2wt percentage was investigated. The methane conversion in this case was below thermodynamic equilibrium compared to previous catalyst used. However, the products selectivity ratio of H_2/CO is in agreement with was obtained in 1wt%-K_2O loading content, which is close to unity.

The low conversion of methane is due to more blockage of nickel stepped active surface site, which is proportional to increase in potassium content present. High loading content of promoter favors increase in stability and decrease in catalytic activity. The stability as shown in Fig 4.22 was observed until after 5 h time on stream and the activity was monitored continuously for 10 h. The H_2/CO ratio followed the same trend as compared to low potassium-loading content, which is suitable for syn-gas, methanol and oxygenated products synthesis.

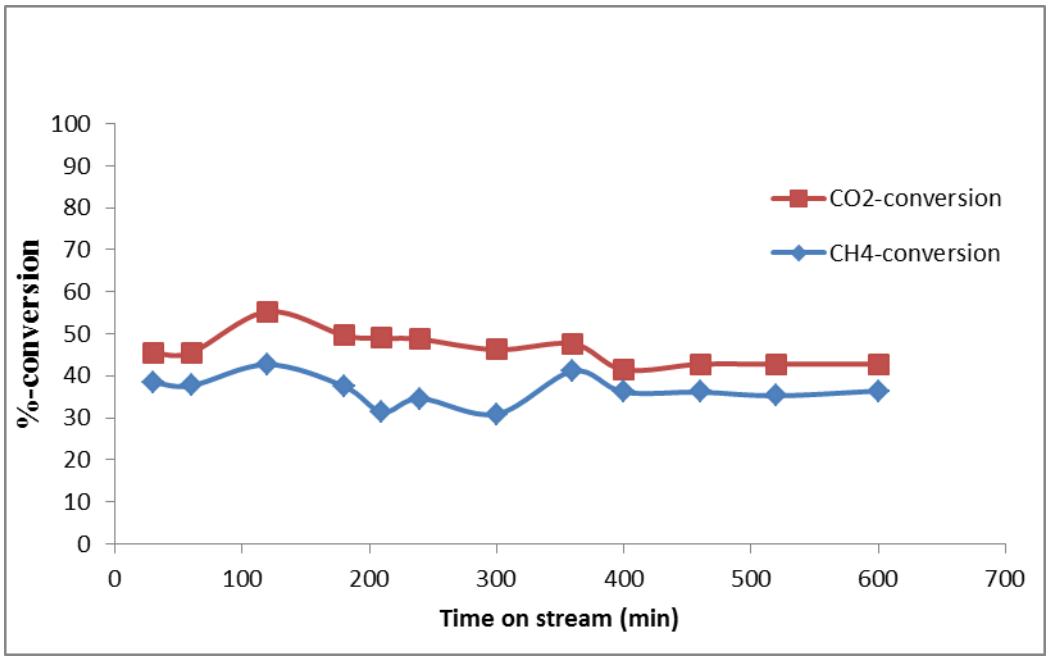

Fig. 4.22: CH_4 and CO_2 conversion with respect to time on stream over 5Ni-2K/CNF-SiC catalyst at 800^oC for dry reforming (CH_4: CO_2= 1:1).

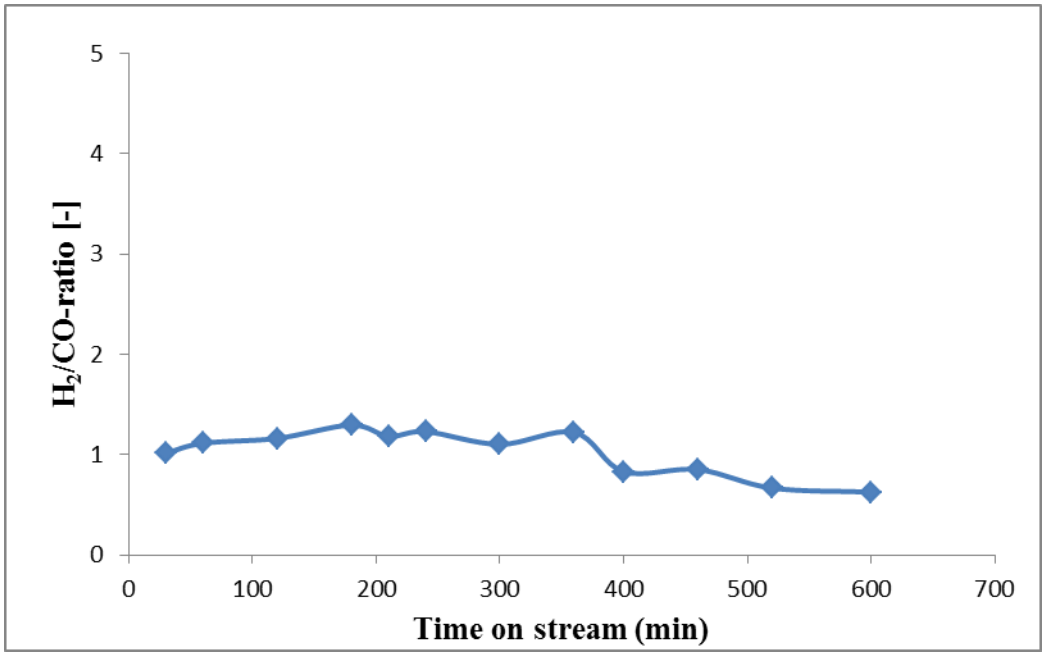

Fig. 4.23: H_2/CO ratio with respect to time on stream over 5Ni-2K/CNF-SiC catalyst at 800^{o}C (CH_4: CO_2= 1:1).

The last catalyst tested for dry reforming was aimed to observe the effect of higher nickel loading by keeping promoter content constant at 1wt%, where stability, conversion and selectivity ratio is moderate. The catalyst 10Ni-1K/CNF-SiC was prepared via co-impregnation of nickel and potassium precursors.

In Fig 4.24, the observed CH_4 and CO_2 conversion was 70% and 75% respectively. The methane conversion is in agreement with thermodynamic equilibrium conversion because of high loading content of nickel. Nevertheless, the CO_2 conversion was higher than CH_4 due to gasification of coke on the catalyst surface. The explanation for methane high conversion is due to presence of more active stepped surface of nickel than close packed terraces, which were not blocked by promoter. This catalyst activity result could also be explained with the one without promoter (10Ni/CNF-SiC) which was highly selective towards H_2 and high conversion of CH_4. However, the CO_2 conversion in this case was different from that of catalyst without promoter.

In contrast with selectivity ratio results obtained with 5Ni-1K/CNF-SiC, the H_2/CO ratio is approximately four (4), which is an indication that this catalyst is selective towards hydrogen than carbon monoxide and suitable for hydrogen production not syngas and methanol synthesis.

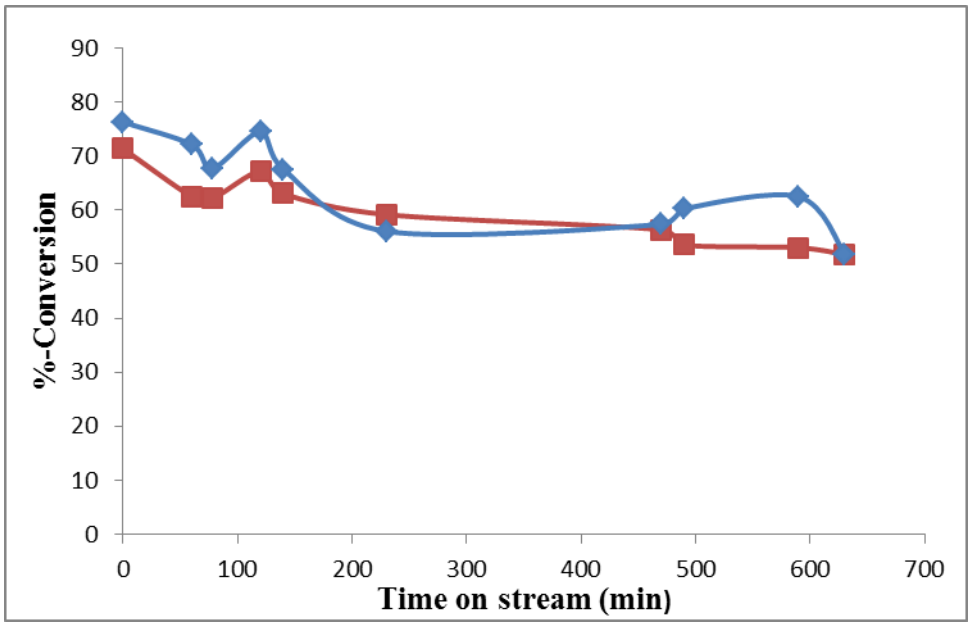

Fig. 4.24: CH_4 and CO_2 conversion with respect to time on stream over 10Ni-1K/CNF-SiC catalyst at 800^oC for dry reforming (CH_4: CO_2= 1:1).

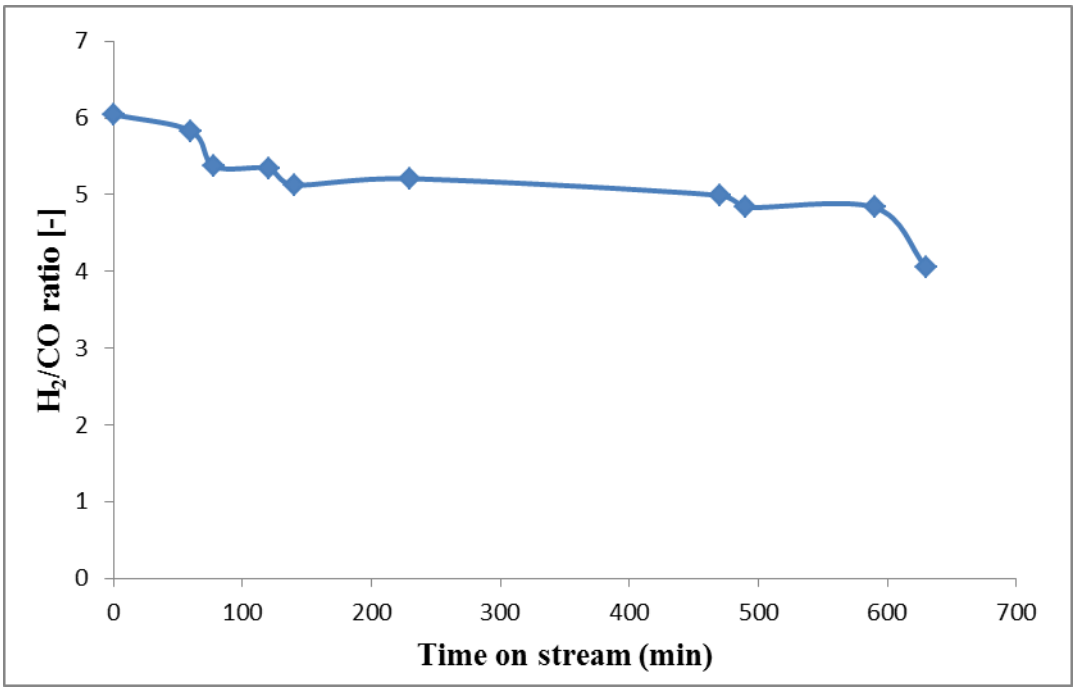

Fig. 4.25: H_2/CO ratio with respect to time on stream over 10Ni-1K/CNF-SiC catalyst at 800^{o}C (CH_4: CO_2= 1:1).

CHAPTER 5

CONCLUSION

Carbon nanofibers (CNFs) of diameter 20-150 nm and carbon nanobulbs of average diameter of 250 nm have been grown at temperature ranges from 600-900^{o}C using Fe and Ni as active catalysts, in a catalytic thermal chemical vapour deposition (C-TCVD) reactor. Due to inert nature of SiC-foam, mesoporous oxide layer was deposited to create oxygen-containing surface for anchoring sites and to enhance the specific surface area. The SEM was employed to examine the morphology and the diameter of as-synthesized carbon nanostructures on 3D SiC-foam at different temperatures. The physiosorption properties were analyzed by N_2 adsorption-desorption isotherm to determine the surface area, pore size and pore volume. The as-synthesized CNFs at 700^{o}C with nickel-based catalyst has the highest surface area. Raman technique was applied to evaluate the degree of graphitization of CNFs synthesized at 700^{o}C.

Generally, both Fe and Ni have high potential to decompose carbon-containing gases to form CNSs on 3-D SiC-foam and expected to perform better as catalyst and/or catalyst support compared to conventional ones, but the as-synthesized carbon nanostructures with Ni-growth shows (i) high external surface area, (ii) high macroporosity (iii) high degree of graphitization than Fe-growth and it is expected to have high thermal conductivity, low tortuosity and efficient mass and heat transfer for catalytic applications.

Nickel-grown CNFs at 700^{o}C, with high specific surface area were applied in catalytic dry reforming of methane at 800^{o}C. Different Ni-loading on the support was prepared

with and without potassium promoter. It was observed that Ni-supported on CNFs without promoter is selective towards hydrogen production with high H_2/CO ratio in all cases, which is not suitable for conversion of syn-gas to methanol, dimethyl ether and other economical valuable products.

The addition of promoter tailored the products towards H_2/CO being approximately unity, which is required from practical point of view to produce syn-gas, methanol, dimethyl ether and valuable oxygenated products.

At high Ni-loading with 1wt%-K, the conversion of CH_4, CO_2 higher, but the selectivity was towards the hydrogen production with high H_2/CO-ratio.

REFERENCES

[1] Cutler Cleveland CMH, Jay Gulledge, J. Emmett Duffy, Andy Jorgensen. "Carbon". In: Encyclopedia of Earth. Eds. Cutler J. Cleveland (Washington, D.C.: Environmental Information Coalition, National Council for Science and the Environment). First published in the Encyclopedia of Earth November 18, 2008; Last revised Date October 3, 2011.

[2] Dresselhaus MS, Dresselhaus G, Eklund PC. Science of fullerenes and carbon nanotubes: their properties and applications: Academic Press; 1996.

[3] Iijima S. Helical microtubules of graphitic carbon. Nature. 1991;354(6348):56-8.

[4] Kroto HW, Heath JR, O'Brien SC, Curl RF, Smalley RE. C60: Buckminsterfullerene. Nature. 1985;318(6042):162-3.

[5] Nasibulin AG, Pikhitsa PV, Jiang H, Brown DP, Krasheninnikov AV, Anisimov AS, et al. A novel hybrid carbon material. Nature Nanotechnology. 2007;2(3):156-61.

[6] Ge M, Sattler K. Observation of fullerene cones. Chemical Physics Letters. 1994;220(3-5):192-6.

[7] Mackay AL, Terrones H. Diamond from graphite [7]. Nature. 1991;352(6338):762.

[8] Itoh S, Ihara S, Kitakami JI. Toroidal form of carbon C360. Physical Review B. 1993;47(3):1703-4.

[9] Amelinckx S, Zhang XB, Bernaerts D, Zhang XF, Ivanov V, Nagy JB. A formation mechanism for catalytically grown helix-shaped graphite nanotubes. Science. 1994;265(5172):635-7.

[10] Humberto T, Mauricio T. Curved nanostructured materials. New Journal of Physics. 2003;5(1):126.

[11] Teo KB, Singh C, Chhowalla M, Milne WI. Catalytic synthesis of carbon nanotubes and nanofibers. Encyclopedia of nanoscience and nanotechnology. 2003;10(1).

[12] De Jong KP, Geus JW. Carbon nanofibers: catalytic synthesis and applications. Catalysis Reviews. 2000;42(4):481-510.

[13] Shea WR, Ruse M. Papers Deriving from the Third International Conference on the History and Philosophy of Science, Montreal, Canada, 1980: Springer; 1983.

[14] Ebbesen TW, Ajayan PM. Large-scale synthesis of carbon nanotubes. Nature. 1992;358(6383):220-2.

[15] Harris PJF. Solid state growth mechanisms for carbon nanotubes. Carbon. 2007;45(2):229-39.

[16] Yakobson BI, Smalley RE. Fullerene nanotubes: C 1,000,000 and beyond. American Scientist. 1997;85(4):324-37.

[17] Guo T, Nikolaev P, Rinzler AG, Tománek D, Colbert DT, Smalley RE. Self-assembly of tubular fullerenes. Journal of Physical Chemistry. 1995;99(27):10694-7.

[18] Dai H, Kong J, Zhou C, Franklin N, Tombler T, Cassell A, et al. Controlled chemical routes to nanotube architectures, physics, and devices. Journal of Physical Chemistry B. 1999;103(51):11246-55.

[19] Fan S, Chapline MG, Franklin NR, Tombler TW, Cassell AM, Dai H. Self-oriented regular arrays of carbon nanotubes and their field emission properties. Science. 1999;283(5401):512-4.

[20] Collins PG, Avouris P. Nanotubes for electronics. Scientific American. 2000;283(6):62-9.

[21] R. Saito GD, and M. S. Dresselhaus, "Physical Properties of Carbon Nanotubes," Imperial College press, London, 1998.

[22] M. F. Yu OL, M. J. Dyer, K. Moloni, T. F. Kelly and R. S. Ruoff, "Strength and breaking mechanism of multiwalled carbon nanotubes under tensile load", Science, Vol. 287, (2000), 287, pp. 637-640.

[23] Wong EW, Sheehan PE, Lieber CM. Nanobeam Mechanics: Elasticity, Strength, and Toughness of Nanorods and Nanotubes. Science. 1997;277(5334):1971-5.

[24] Toebes ML, Bitter JH, van Dillen AJ, de Jong KP. Impact of the structure and reactivity of nickel particles on the catalytic growth of carbon nanofibers. Catalysis Today. 2002;76(1):33-42.

[25] Chinthaginjala JK, Seshan K, Lefferts L. Preparation and Application of Carbon-Nanofiber Based Microstructured Materials as Catalyst Supports. Industrial & Engineering Chemistry Research. 2007;46(12):3968-78.

[26] Mukul Kumar (2011). Carbon Nanotube Synthesis and Growth Mechanism CN-S, Characterization, Applications, Dr. Siva Yellampalli (Ed.), ISBN: 978-953-307-497-9.

[27] Andrew SPS. Heterogeneous Catalyst Preparation: The Fabrication of Microstructures. 1976, p. 429-48.

[28] PEREGO C, VILLA P. Catalyst preparation methods. Catalysis Today. 1997;34(3-4):281-305.

[29] Haber J, Block J, Delmon B. Manual of methods and procedures for catalyst characterization. Pure and applied chemistry. 1995;67:1257-.

[30] Deleuze H, Backov R. Integrative Chemistry Routes toward Advanced Functional Hierarchical Foams. Hierarchically Structured Porous Materials. 2011.

[31] Inayat A, Freund H, Zeiser T, Schwieger W. Determining the specific surface area of ceramic foams: The tetrakaidecahedra model revisited. Chemical Engineering Science. 2011;66(6):1179-88.

[32] Inayat A, Schwerdtfeger J, Freund H, Körner C, Singer RF, Schwieger W. Periodic open-cell foams: Pressure drop measurements and modeling of an ideal tetrakaidecahedra packing. Chemical Engineering Science. 2011;66(12):2758-63.

[33] ZHANG J-y, FU Y-m, ZENG X-m. Compressive properties of open-cell ceramic foams. Transactions of Nonferrous Metals Society of China. 2006;16:s453-s6.

[34] Saggio-Woyansky J, Scott CE, Minnear W. Processing of porous ceramics. American Ceramic Society Bulletin. 1992;71(11):1674-82.

[35] Colombo P. Ceramic foams: fabrication, properties and applications. Key Engineering Materials. 2001;206:1913-8.

[36] Lange F, Miller K. Open-cell, low-density ceramics fabricated from reticulated polymer substrates. Advanced Ceramic Materials;(USA). 1987;2(4).

[37] Sepulveda P. Gelcasting foams for porous ceramics. American Ceramic Society Bulletin. 1997;76(10):61-5.

[38] Twigg M, Richardson J. Theory and applications of ceramic foam catalysts. Chemical Engineering Research and Design. 2002;80(2):183-9.

[39] Twigg MV, Richardson JT. Fundamentals and applications of structured ceramic foam catalysts. Industrial & Engineering Chemistry Research. 2007;46(12):4166-77.

[40] Ichi-oka H-a, Higashi N-o, Yamada Y, Miyake T, Suzuki T. Carbon nanotube and nanofiber syntheses by the decomposition of methane on group 8–10 metal-loaded MgO catalysts. Diamond and Related Materials. 2007;16(4–7):1121-5.

[41] Rodríguez-reinoso F. The role of carbon materials in heterogeneous catalysis. Carbon. 1998;36(3):159-75.

[42] Rodriguez NM. A review of catalytically grown carbon nanofibers. Journal of Materials Research. 1993;8(12):3233-50.

[43] Gu JY, Li KX, Wang J, He HW. Control growth of carbon nanofibers on Ni/activated carbon in a fluidized bed reactor. Microporous and Mesoporous Materials. 2010;131(1–3):393-400.

[44] Serp P. Carbon Nanotubes and Nanofibers in Catalysis. Carbon Materials for Catalysis: John Wiley & Sons, Inc. 2008, p. 309-72.

[45] Ledoux M-J, Pham-Huu C. Carbon nanostructures with macroscopic shaping for catalytic applications. Catalysis Today. 2005;102–103(0):2-14.

[46] Pham-Huu C, Ledoux M-J. Carbon nanomaterials with controlled macroscopic shapes as new catalytic materials. Top Catal. 2006;40(1-4):49-63.

[47] Nguyen DL, Leroi P, Ledoux MJ, Pham-Huu C. Influence of the oxygen pretreatment on the CO2 reforming of methane on Ni/β-SiC catalyst. Catalysis Today. 2009;141(3–4):393-6.

[48] Treacy D, Ross JR. The potential of the CO2 reforming of CH4 as a method of CO2 mitigation. A thermodynamic study. Prepr Pap-Am Chem Soc, Div Fuel Chem. 2004;49(1):126.

[49] Aresta M, Tommasi I. Carbon dioxide utilisation in the chemical industry. Energy Conversion and Management. 1997;38:S373-S8.

[50] Centi G, Perathoner S. Opportunities and prospects in the chemical recycling of carbon dioxide to fuels. Catalysis Today. 2009;148(3–4):191-205.

[51] Thakur DB, Tiggelaar RM, Gardeniers JGE, Lefferts L, Seshan K. Carbon nanofiber based catalyst supports to be used in microreactors: Synthesis and characterization. Chemical Engineering Journal. 2010;160(3):899-908.

[52] Albarazi A, Beaunier P, Da Costa P. Hydrogen and syngas production by methane dry reforming on SBA-15 supported nickel catalysts: On the effect of promotion by Ce0.75Zr0.25O2 mixed oxide. International Journal of Hydrogen Energy. 2013;38(1):127-39.

[53] Bhattacharyya A, Chang VW, Schumacher DJ. CO2 reforming of methane to syngas: I: evaluation of hydrotalcite clay-derived catalysts. Applied Clay Science. 1998;13(5):317-28.

[54] Rezaei M, Alavi S, Sahebdelfar S, Yan Z-F. Syngas production by methane reforming with carbon dioxide on noble metal catalysts. Journal of Natural Gas Chemistry. 2006;15(4):327-34.

[55] Kang K-M, Kim H-W, Shim I-W, Kwak H-Y. Catalytic test of supported Ni catalysts with core/shell structure for dry reforming of methane. Fuel Processing Technology. 2011;92(6):1236-43.

[56] Z. Xu YL, J. Zhang, L. Chang, R. Zhou, Z. Duan, Bound-state Ni species—a superior form in Ni-based catalyst for CH4/CO2 reforming, Appl. Catal. A Gen. 210 (2001) 45–53.

[57] Ni J, Chen L, Lin J, Kawi S. Carbon deposition on borated alumina supported nano-sized Ni catalysts for dry reforming of CH 4. Nano Energy. 2012;1(5):674-86.

[58] Wang W, Stagg-Williams SM, Noronha FB, Mattos LV, Passos FB. Partial oxidation and combined reforming of methane on Ce-promoted catalysts. Catalysis Today. 2004;98(4):553-63.

[59] Jing QS, Zheng XM. Combined catalytic partial oxidation and CO2 reforming of methane over ZrO2-modified Ni/SiO2 catalysts using fluidized-bed reactor. Energy. 2006;31(12):1848-56.

[60] Özkara-Aydınoğlu Ş, Özensoy E, Aksoylu AE. The effect of impregnation strategy on methane dry reforming activity of Ce promoted Pt/ZrO2. International Journal of Hydrogen Energy. 2009;34(24):9711-22.

[61] Barroso-Quiroga MM, Castro-Luna AE. Catalytic activity and effect of modifiers on Ni-based catalysts for the dry reforming of methane. International Journal of Hydrogen Energy. 2010;35(11):6052-6.

[62] Luisetto I, Tuti S, Di Bartolomeo E. Co and Ni supported on CeO2 as selective bimetallic catalyst for dry reforming of methane. International Journal of Hydrogen Energy. 2012;37(21):15992-9.

[63] Ranjbar A, Rezaei M. Dry reforming reaction over nickel catalysts supported on nanocrystalline calcium aluminates with different CaO/Al2O3 ratios. Journal of Natural Gas Chemistry. 2012;21(2):178-83.

[64] Ranjbar A, Rezaei M. Preparation of nickel catalysts supported on CaO.2Al2O3 for methane reforming with carbon dioxide. International Journal of Hydrogen Energy. 2012;37(8):6356-62.

[65] Juan-Juan J, Román-Martínez MC, Illán-Gómez MJ. Effect of potassium content in the activity of K-promoted Ni/Al2O3 catalysts for the dry reforming of methane. Applied Catalysis A: General. 2006;301(1):9-15.

[66] Yang H, Coombs N, Sokolov I, Ozin GA. Free-standing and oriented mesoporous silica films grown at the air-water interface. Nature. 1996;381(6583):589-92.

[67] Yu X, Lin B, Gong B, Lin J, Wang R, Wei K. Effect of nitric acid treatment on carbon nanotubes (CNTs)-cordierite monoliths supported ruthenium catalysts for ammonia synthesis. Catalysis Letters. 2008;124(3-4):168-73.

[68] Zhang C, Li J, Liu E, He C, Shi C, Du X, et al. Synthesis of hollow carbon nano-onions and their use for electrochemical hydrogen storage. Carbon. 2012;50(10):3513-21.

[69] Somani PR, Umeno M. Importance of transmission electron microscopy for carbon nanomaterials research. Modern Research and Educational Topics in Microscopy. 2007(3):634-42.

[70] Martin-Gullon I, Vera J, Conesa JA, González JL, Merino C. Differences between carbon nanofibers produced using Fe and Ni catalysts in a floating catalyst reactor. Carbon. 2006;44(8):1572-80.

[71] Rodriguez NM, Chambers A, Baker RTK. Catalytic engineering of carbon nanostructures. Langmuir. 1995;11(10):3862-6.

[72] Zhao N, Cui Q, He C, Shi C, Li J, Li H, et al. Synthesis of carbon nanostructures with different morphologies by CVD of methane. Materials Science and Engineering A. 2007;460-461:255-60.

[73] Liu CG, Fang HT, Li F, Liu M, Cheng HM. Single-walled carbon nanotubes modified by electrochemical treatment for application in electrochemical capacitors. Journal of Power Sources. 2006;160(1):758-61.

[74] Tribolet P, Kiwi-Minsker L. Palladium on carbon nanofibers grown on metallic filters as novel structured catalyst. Catalysis Today. 2005;105(3–4):337-43.

[75] Jeet K, Jindal VK, Bharadwaj LM, Avasthi DK, Dharamvir K. Damaged carbon nanotubes get healed by ion irradiation. Journal of Applied Physics. 2010;108(3):034302-6.

[76] Ruch PW, Hardwick LJ, Hahn M, Foelske A, Kötz R, Wokaun A. Electrochemical doping of single-walled carbon nanotubes in double layer capacitors studied by in situ Raman spectroscopy. Carbon. 2009;47(1):38-52.

[77] Bengaard HS, Alstrup I, Chorkendorff I, Ullmann S, Rostrup-Nielsen JR, Nørskov JK. Chemisorption of methane on Ni(100) and Ni(111) surfaces with preadsorbed potassium. Journal of Catalysis. 1999;187(1):238-44.

[78] Bengaard HS, Nørskov JK, Sehested J, Clausen BS, Nielsen LP, Molenbroek AM, et al. Steam reforming and graphite formation on Ni catalysts. Journal of Catalysis. 2002;209(2):365-84.

[79] San José-Alonso D, Illán-Gómez MJ, Román-Martínez MC. K and Sr promoted Co alumina supported catalysts for the CO2 reforming of methane. Catalysis Today. 2011;176(1):187-90.

Vitae

Name: Saheed Adewale Ganiyu

Nationality: Nigerian

Date of Birth: 8/8/1981

Email: gsadewale@gmail.com

Address: Chemistry Dept. King Fahd University of petroleum and Minerals, P.O. Box 31261, Dhahran, Saudi Arabia.

Academic Background: B.Sc. Industrial Chemistry, 2005 University of Ilorin, Ilorin Nigeria.